International Journal of Engineering Works
https://www.ijew.io/
ISSN-p: 2521-2419
ISSN-e: 2409-2770
Vol. 11, Issue 04, PP. 61-104, April 2024
https://doi.org/10.34259/ijew.24.110461104

Polymer Composite Materials for Electromagnetic Waves Absorption

W. H. Nishani De Soyza[1], Alfadil Yousif[2], Junliang Liu[3]
[1,2,3]Department of Chemistry and Chemical Engineering, Yangzhou University, China
3351778834@qq.com[1], alfadil@163.com[2], liujunliang@yzu.edu.cn[3]
Received: 27 January, Revised: 11 April, Accepted: 13 April

***Abstract*—**Electromagnetic wave absorption materials play a vital role in the medical materials field. On the other hand, due to the various adverse effects on humans and other species by military applications and environmental factors, electromagnetic pollution management and interference of electromagnetic have received much attention recently. Specifically, EM-wave absorbers (EMWAs) could minimize the Radar Signature of Structures (RCS), hence decreasing the likelihood of radar detection. The interaction of electromagnetic (EM) waves of various sources can cause machine malfunction owing to data misinterpretation or accidental deletion. Because of the thickness and weight constraints, structural materials that are both light and strong, improved possibilities for electromagnetic absorption are required. In this work, the progression, characterization, and process technology of polymer composite materials used in EMI shielding or EM wave absorption applications were sought. Characterization of EM wave absorption potential was conducted using all the methods and theories. Single and multilayered combinations of surface-modified polymers, EM wave interaction features, and design ideas for efficient broadband EM wave absorption were studied. Polymer composite materials have been reviewed for the past 10 years in overseas and domestic(China) articles. To anticipate EM wave transmission, reflection, and therefore absorption, a computer-aided method has also been presented. Estimated results were verified and compared by reviewing process methods and material performance analysis.

***Keywords*—** Polymer Composites; Electromagnetic Waves Absorption; Electromagnetic Interference; Electromagnetic Waves Shielding.

I. INTRODUCTION

Throughout this article, beginning with the next chapter, essential concepts of electromagnetic wave theory and facts about electromagnetic wave absorption are provided. Here discuss the benefits of the created EM wave-absorbing polymer composite materials by evaluating contemporary polymer composite materials and their electromagnetic absorption capabilities and process methods over the past ten years and future developments. The third chapter discusses the overall summary and outlook. These sections contain information on the electromagnetic characterization of a review of polymer composite materials of overseas and domestic articles. create these components, incorporating the applicable criteria that follow.

A. The direction of study

Applications of EM wave absorption seek to reduce incident EM energy. The material's EM energy is lost as heat. Earlier instances of EMI shielding utilized geometrical designs to disperse the electromagnetic energy carried by incident waves, resulting in loss of reflection. Due to the difficulties associated with the uncontrolled weight, thickness, and shape of EMW absorption materials, research has concentrated on modifying the magnetic and dielectric characteristics of suitable materials such as polymer composites. Apart from thickness and weight, frequency efficacy has been taken into account. Using multilayered structures, the demand for EM wave absorbents that are effective over a broad frequency range has been met.

The purpose of this project is to investigate polymer composite materials that absorb or protect electromagnetic radiation. Numerous ways of material application affected the complex magnetic and dielectric characteristics of polymer composite materials. We evaluated the influence of surface modification on EM wave reflection, transmission, and absorption. This work will direct to an understanding of the EMW absorption mechanism and characterization of polymer composite materials of EMW absorption in the past few years.

B. The Development of History

Following the invention of electromagnetic theory, electromagnetic (EM) wave-based devices became widely used in engineering applications. Electromagnetic waves with certain wavelengths released by power sources are utilized for a variety of purposes, including wireless transfer of information, broadcasting, biomedical imaging, and foreign object identification. Electromagnetic waves, because of their interaction with the atmospheric air, can be used to transmit data between remote terminals such as satellites and space shuttles.

Historically, electromagnetic wave absorption materials were used primarily to reduce the radar cross-sections of military vehicles. Following the invention of materials capable of absorbing electromagnetic waves at a given frequency, multi-frequency radar-absorbing and jamming devices were developed. The advancement of technology has resulted in a rise in the widespread use of methods that rely on electromagnetic radiation in everyday applications. Consequently, developing efficient necessity for broadband electromagnetic wave absorbers has arisen. Earlier alternatives, such as Jaumann multilayered absorbers, had drawbacks, including increased thickness and weight. The key to resolving such issues is mostly

through the change of polymer composite materials' fundamental qualities. [1]

C. *The current situation*

The growing demand for EM wave-based technologies has resulted in widespread service issues applications in engineering. Interfering with electromagnetic waves from various references causes misunderstanding of the statistics delivered utilizing electromagnetic waves. As an outcome, the creation of shielding or absorbing structures was already a requirement for eradicating electromagnetic interference (EMI) and ensuring data security. Additionally, EM waves are employed in military and commercial applications for "radio detection and ranging" (RADAR). The development of radar applications has concentrated on high-resolution projection at a sufficiently long range. Electronic, geometric, and Materials Engineering methods were utilized to lessen radar cross-section (RCS). Additional components connected to the main body of a system wreak havoc on the performance of mobile mechanisms. Consequently, the manufacturing together with the advancement of EM wave absorption polymer composite elements with structural properties became strategically important, particularly for military, medical, and civil applications[2].

D. *Forecast*

Electromagnetic interference (EMI) is a disruption that occurs when an object is subjected to electromagnetic induction or radiation released by an outside source.[3] Numerous researchers have focused on polymer composites for EMI shielding purposes. This is mostly due to their attributes, which typically consist of low density, superior electromechanical capabilities, thermal stability, and wide dimension, as well as unique and less frequent traits, such as electromagnetic absorption. Additionally, these materials solve the shortcomings connected with the usage of metallic materials, such as lightweight, flexibility, corrosion resistance, and processing complexity.[4]

Further research is being conducted towards the development of polymer composite materials for electromagnetic absorption. utilizing cutting-edge technology, such as computational and simulation engineering techniques.

II. CONTENT

The foundations of electromagnetic (EM) waves and their absorption methods and research progress over the past ten years and future predictions are covered in this chapter. First, the fundamental features of electromagnetic waves will be presented**.**

A. *History and fundamental methods analysis of electromagnetic wave absorption*

James Clerk Maxwell, a Scottish scientist, is the first to unify the fundamental rules of electromagnetic waves. The Maxwell Equations for comprehension and utilizing electromagnetic wave characteristics (EM wave) were devised to unify the phenomena of electricity and magnetism. Equations of Maxwell's are numerical representations of the laws of Gauss, Ampere, and Faraday. Electromagnetic waves travel across open space at 3.00 x 10^8 m/s, corresponding to the observed speed of light (c). The equation expresses the frequency (f) and wavelength (λ) of an electromagnetic wave.[1]

$$c = \lambda f \tag{1}$$

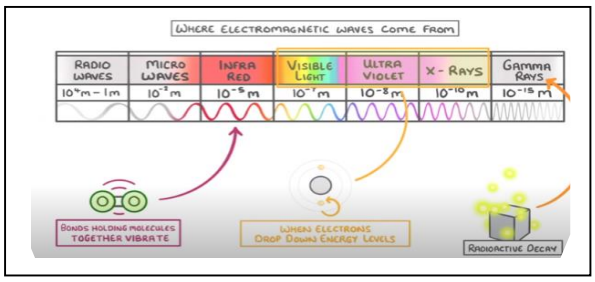

Figure 1. Electromagnetic spectrum

Absorption of electromagnetic waves is a procedure wherein the power/energy contained in the wave has subsided and subsequently turned to another type of energy, like thermal energy. Therefore, the wave cannot be reflected or penetrated through the substances. Three processes occur once electromagnetic radiation is impacted on a substance: reflection, absorption, and penetration.[5],[6]

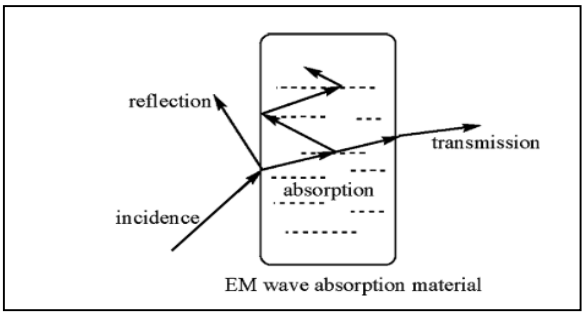

Figure 2. The general process of an incident EM wave through an EM absorption material

As excellent absorption materials for EM waves, they are required to meet two essentials:

(1) Impedance matching between free space and the substrate surfaces to avoid wave reflection, necessitating complex permittivity near complex permeability

(2) Materials should absorb as many incoming waves as feasible within absorbers, necessitating high magnetic and/or dielectric loss.

The potential of electromagnetic waves to absorb energy was frequently illustrated by the reflection loss (R_L): R_L values of 10 and 20 dB indicate that 90 and 99 percent, respectively, of EM waves were absorbed mostly by materials. The mechanism of energy depletion is mostly dielectric and magnetic loss.[5]

$$RL = 20 \log \left| \frac{Z_{in} - 1}{Z_{in} + 1} \right| \tag{2}$$

Mechanism of magnetic loss

Three forms of energy loss occur when magnetic material interacts with an electromagnetic wave: magnetic hysteresis loss, eddy current loss, and residual loss. In low magnetic flux densities and lower frequencies, the magnetic loss may indeed be stated mathematically. Using Legg's equation, where a, e, c, μ, B, and $t_g\delta m$ denote the magnetic hysteresis coefficient, eddy current loss coefficient, residual loss, permeability, magnetic flux density, and magnetic loss tangent, respectively.[5],[7],[8]

$$\frac{2\pi t_g \delta_m}{\mu} = ef + aB + c \quad (3)$$

Eddy current loss

When a conducting substance is exposed to a magnetic field with alternating magnetic flux, a near-induced voltage is generated including inside the substance dissipating the energy, which is referred to as loss of eddy current. The eddy current reduction coefficient, e, can indicate the eddy current loss with low magnetic flux density and low frequency. The coefficient of eddy current loss may be stated as for electrical conductivity and a sheet having a thickness of d.[9]

$$e = \frac{4\pi^2 \mu_0 d^2 \sigma}{3} \quad (4)$$

According to Eq.(4) a material's thickness and conductivity must be considered to enhance eddy current loss. However, high-conductivity materials would render the permeability unstable at high frequencies.

Magnetic hysteresis loss

Magnetic hysteresis loss is generated by irreversible domain motion and magnetic moment spinning in magnetic materials. The coefficient of magnetic hysteresis is minimal at low magnetic flux concentrations.

$$a = \frac{8b}{3\mu_0 \mu^3} \quad (5)$$

Where μ_0,b, and μ denote the vacuum permeability, the Rayleigh constant, and the material permeability, respectively.[10]

According to (Equation 5) the Loss of magnetic hysteresis is mostly determined by the material's magnetic characteristics, particularly the permeability and rayleigh constant a.[5]

Residual loss

The term "residual loss" pertains to all magnetic losses other than magnetic hysteresis and eddy current. At low frequencies, the residual loss remained mostly due to magnetic aftereffects, such as the thermodynamic instability or hysteresis of certain ions and electrons adjusting to their position of balance regarding the diffusion of the given magnetic field. This is the form of loss, dictated by the variable magnetic field's the material's relaxation period and amplitude. At a staggering rate, ferromagnetic resonance, size resonance, domain wall resonance, and natural resonance, all contribute to the residual deficits. The principles outlined illustrated, that magnetic material anisotropy, optimizing particle size, and other electromagnetic characteristics may result in acceptable magnetic loss. [5],[10],[11]

Dielectric strength loss

When an electromagnetic wave interacts with a dielectric substance, the medium dissipates electric energy, which is subsequently converted to thermal energy; this energy is referred to as dielectric loss. dielectric relaxation loss ($tg\delta_{rel}$), conductance loss ($tg\delta_c$), resonance loss ($tg\delta_{res}$), and others are all causes of dielectric loss.

Conductance loss

If an oscillating current field interacts with a wave absorption material with a specific conductivity, the material produces a conductance current, which eventually dissipates the energy as heat. Consequently, conduction loss is governed by the electric conductivity of the material, which is expressed by the conductivity loss tangent., tgδc.

$$t_g\delta_c = 1.8 \times 10^{10} \frac{\sigma}{f\varepsilon_r} \quad (6)$$

Loss of dielectric relaxation

Under an electric field, the material becomes polarized, but if the rate of polarization change is lower than the change in an electric field results in dielectric relaxation loss. Polarization encompasses a variety of phenomena, including electronic displacement polarization, dipole rotation polarization, ion polarization, and thermal ion polarization. Because The time necessary for electronic dislocation and ion polarizability is only 10-15/10-14 s, and only at extremely high frequencies can these polarizations cause energy loss; whereas, the time required considering dipole rotation and thermal ion polarization, is: approximately 10-8/10-2 s. Therefore, dipole rotation and thermal ion polarization contribute far more to high-frequency relaxation loss. Use the Debye equation to calculate the dielectric relaxation loss tangent, $tg\delta_{rel}$.

$$t_g\delta_{rel} = \frac{\varepsilon''r(\omega)}{\varepsilon' r(\omega)} = \frac{(\varepsilon_{rs} - \varepsilon_{r\infty})\omega\tau}{\varepsilon_{rs} + \varepsilon_{r\infty}\omega^2\tau^2} \quad (7)$$

Loss of resonance and other types of loss

The resonance loss is caused by not only the oscillation of ions, atoms, or electrons inside the medium of radiation absorption, that happens between infrared and ultraviolet frequencies.

Per the explanation above, the magnetic and electronic characteristics, structure of the material, size of the material, morphology, and all have a significant effect on the property of electromagnetic radiation absorbance. Optimizing the material's electromagnetic radiation absorption capability requires careful tuning of all parameters to establish impedance matching. Following that, we shall explore the primary elements impacting the material's wave absorption property.

Complex permeability and permittivity are fundamental electromagnetic properties.

The initial electric variable is a material's relative complex permittivity, which is one of the fundamental properties of the substance. Whereas if the source is utilized as a wave's absorbent, the dielectric loss tangent, indicates the wave absorption effect is more effective the higher the imaginary fraction of complicated permittivity. As an outcome, high-permittivity materials are selected for function as electromagnetic wave absorbers. Alternatively, the reflection component of the wave is rather big for materials with an excessive permittivity, implying that we may pick a permittivity that is appropriate for the application. If somehow the element is a matrix, as a polymer, a material with low dielectric loss is favored for wave absorption. Feature, as it allows for more wave transmission inside the absorbent.[5],[12]

The alternative is complex permeability. Fundamental quantity that affects a material's electromagnetic wave absorption property. We may also derive tgδm = l00/l0 from the electromagnetic loss tangent and the magnetic loss mechanisms that the higher the image component of complex permeability and the smaller the real component, the higher the magnetic loss for wave-absorbing material. When the permeability and permittivity of the material are identical, no electromagnetic wave absorption or reflection effect is optimal.

Conductivity of electricity

According to the mentioned wave absorption mechanisms, rising conductivity results in a rise in conductance losses and eddy current. Nevertheless, because the impedance of materials with high conductance is very minimal in comparison to that, the skin depth and air are quite shallow, but almost all electromagnetic waves are reflected by the components.[5]

Complex permeability and permittivity explain how EM radiation interacts with a substance. The imaginary components of complex permittivity and permeability indicate the loss or dissipation of dielectric and magnetic energy within a substance. The loss tangent of complex permittivity and permeability is the imaginary to real components (energy dissipated). Greater imaginative portions of complex permeability and permittivity allow for greater absorption of electromagnetic waves.[13]

The nano-effect

Nanoscale material possesses exceptional electric, magnetic, and optical capabilities as a consequence of its surface, unique size, and quantum tunnel impact. For example, nanostructures have a lower density than bulk materials; they have a higher specific surface area, which results due to contact polarization and a significant number of active atoms at the material's surface, the interface dielectric loss is considerable. On the other hand, metal magnetic materials conductivity is excessive, resulting in a decrease in excellent permeability at high frequencies generated by electromagnetic wave-induced eddy current loss. When the particle size is less than the skin depth, eddy current loss might occur., which can improve the stability of the wave's absorption quality. Because the skin's thickness of most materials is around 1 μm broadband frequency (10 GHz), nanoparticles will exhibit good Absorption of electromagnetic wave radiation characteristics spanning a broad frequency spectrum [5].

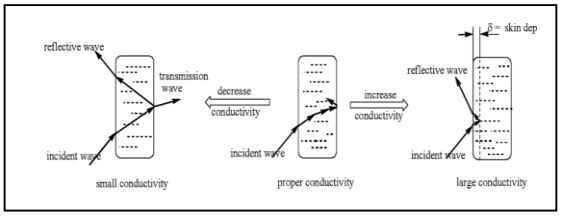

Figure 3. The electromagnetic wave transmission model for materials with different conductivity

Material structure

It is well-known that it is difficult to accomplish impedance matching and wide frequency wave absorption with a magnetic or single dielectric material, due to Snoek's limit of material permeability values below five at GHz frequencies. Thus, it is required to create materials with a variety of multilayer structures, core/shell structures, and mixtures of diverse dielectric and magnetic materials to provide the finest electromagnetic radiation absorption capabilities. Mechanical blends are the most practicable way of preparing composites since they combine magnetic and dielectric material particles directly. The second method is to use a multilayer structure to match the wave impedance, increase electromagnetic wave absorption capabilities, and widen the absorption frequencies of wave absorption material. The fundamental multilayer structure consists of three layers: an electromagnetic wave loss layer, an impedance matching layer, and a reflective layer. By regulating the complicated permittivity and permeability of the material, the impedance layer transmits electromagnetic waves without reflection. In the electromagnetic radiation loss layer, which is formed of high dielectric or magnetic loss materials, the electromagnetic wave is depleted. Due to the material's unique structure, it exhibits superior absorption of electromagnetic wave radiation capability and may be employed at a variety of frequencies by altering the impedance match range. Another technique of matching impedance is to combine incorporating not just the multilayer structure of electromagnetic materials, but also the homogenous dispersion of nanoparticles inside wave absorption materials, are the two techniques. Therefore, the material having a core/shell structure may exhibit higher electromagnetic wave absorption capabilities.[5]

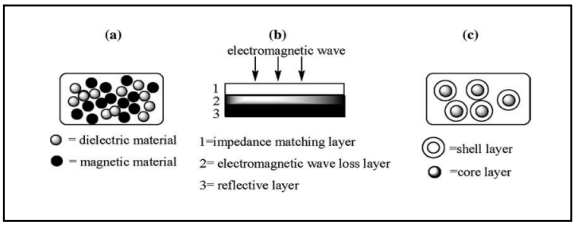

Figure 4. EM absorption material layer types

The free-space approach is an approach for determining complicated EM parameters as well as the reflection and transmission characteristics of electromagnetic waves in material under a certain thickness. Free-space methodology's main advantage is that it may be used on inhomogeneous and/or anisotropic material. The free-space arrangement used in this investigation is schematically depicted in Figure 5.

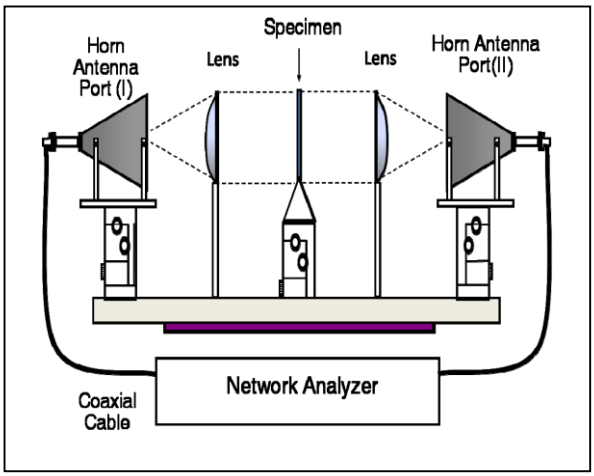

Figure 5. Schematic of the free-space measurement setup

The free-space method is widely considered a useful technique for determining the electromagnetic characteristics of inhomogeneous materials including composites and ceramics. Additionally, because the free-space approach is contactless and non-destructive, it is useful for describing irregularly shaped and delicate materials.[1]

B. Review analysis

1) Current situation of overseas research

Polyaniline Conducting Composites EMW Absorbers.

Conducting polymers are superior absorbers of microwave radiation due to their technical advances over electromagnetically absorbent inorganic materials, including their ease of processing, lightweight, capability to change their electromagnetic properties depending on their nature, dopant concentration, synthesis conditions, and so on.[14]

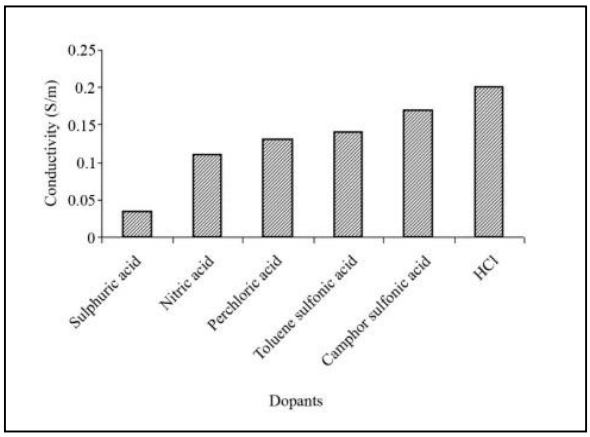

Figure 6. Effect of different dopants on the conductivity of PAN in pellet form

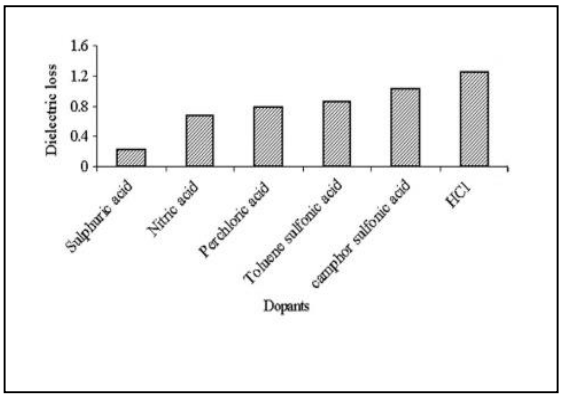

Figure 7. Effects of different dopants on the dielectric loss of PAN in pellet form

Process: The in-situ polymerization of aniline in the existence of polyvinyl chloride emulsified grade. resulted in the formation of cyclohexanone soluble conducting PAN composites with a microwave conductivity measuring 12.5 S/m. The dielectric characteristics of composite materials were examined. The microwave radiation absorption characteristics of the composites were reviewed throughout a range of frequency bands, including bands S, C, and X (2–12 GHz). the coefficient of absorption was determined to be over 200 m^{-1}, suggesting that may be utilized to fabricate microwave radiation absorbers for sensing applications.[14]

When the polar group is big or the medium has a high viscosity, the molecule's rotatory motion is insufficiently quick to achieve equilibrium with the field. The size of the HCl dopant is less than that of any other dopant. [15],[16]

Table 1. Dielectric properties of 1:1.5 PANI: PVC composite at S, C, and X bands

[1]	[2] S band (2.97 GHz)	[3] C band (7.56 GHz)	[4] [5] X band (10.97 GHz)
[6] Dielectric loss	[7] 76	[8] 0.331	[9] 0.6
[10] Conductivity (S/m)	[11] 12.549	[12] 0.141	[13] 0.4
[14] Dielectric constant	[15] 4.18	[16] 0.76	[17] 2.84
[18] Dielectric heating coefficient (ln J)	[19] 0.0122	[20] 0.153	[21] 1.22

Table 2. Absorption coefficient and skin depth of PANI: PVC composite at S-band (at 2.97 GHz)

	Composition (Pani:PVC)		
Property	2:1	1:1 1:2	1:1.5
Absorption coefficient (m^{-1})	29.9	57.6 30	235
Skin depth (m)	0.03	0.02 0.031	0.004

Due to the coefficient of absorption is derived from complex permittivity and is a measurement of absorption of electromagnetic waves as they pass through a substance, dielectric materials have been classed according to this characteristic, which indicates the transparency of passing waves.

Nanocrystalline FeCuNbSiB alloy flake/polymer composite sheets of varying flake thickness

The influence of magnetic alloy flake thicknesses on electromagnetic radiation absorption characteristics of nanocrystals $Fe_{73.5}Cu_1Nb_3Si_{15.5}B_7$(atw%) alloy polymer/flakes composite sheets that can be accessed in the quasi-microwave range were presented. The thickness was reduced from 18 to 1-2 m after 24 hours of attrition milling. The composite sheet with milled alloy flakes demonstrated significantly improved power loss characteristics across the band range in comparison to the sheet containing unmilled alloy flakes. Notwithstanding a notable increase in electromagnetic loss proportional to milling time was found in the restricted frequency band of 4 to 6 gigahertz, complex permeability had a relatively little influence on flake thickness. The complex permittivity, on the other hand, rose significantly extending the milling time, and a strong correlation was identified between the frequency dependency and milling time of the composite sheets' complicated permittivity and power loss. The enhanced electromagnetic radiation absorbance capabilities of composite sheets formed of very thin FeCuNbSiB alloy flake can be attributed to their increased complex permittivity and therefore reduced loss of dielectric.[17]

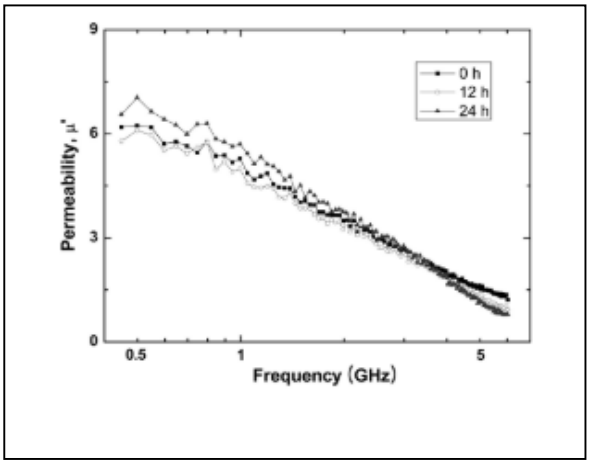

Figure 8. Frequency dependence of the real part of the complex permeability (μ') for the composite sheets including the nanocrystalline FeCuNbSiB alloy flakes milled for 0, 12, and 24 h, respectively

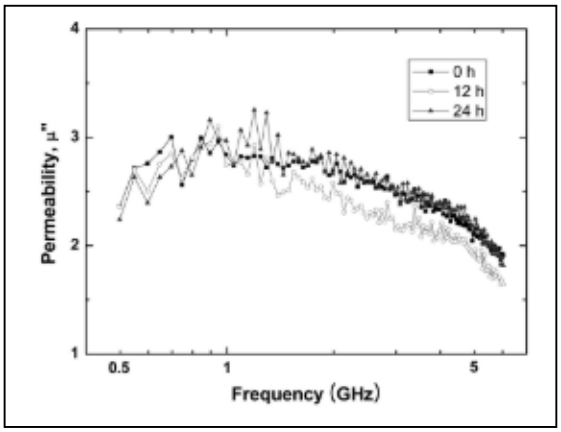

Figure 9. Frequency dependence of the imaginary part of the complex permeability (μ") for the composite sheets including the nanocrystalline FeCuNbSiB alloy flakes milled for 0, 12, and 24 h, respectively

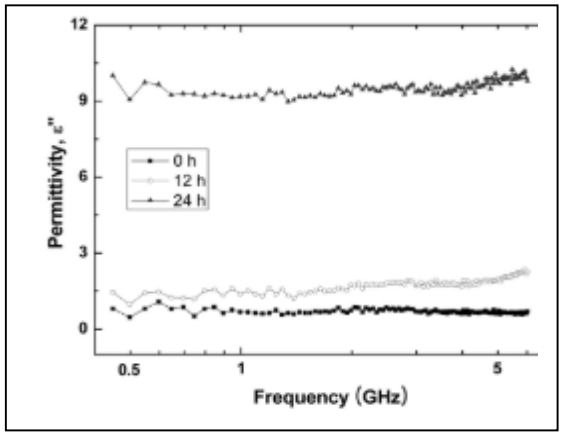

Figure 10. Frequency dependence of the imaginary part of the complex permittivity (ε") for the composite sheets including nanocrystalline FeCuNbSiB alloy flakes milled for 0, 12, and 24 h, respectively

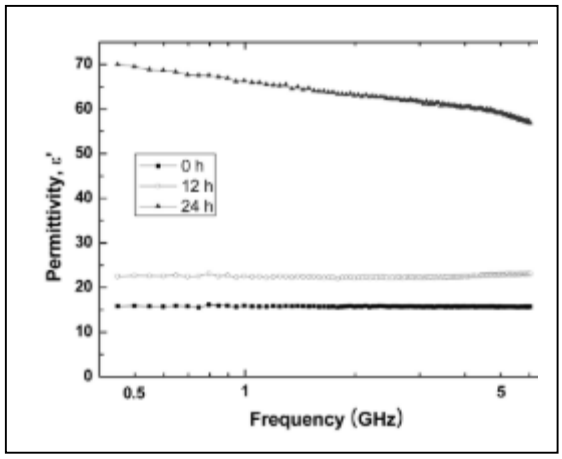

Figure 11. Frequency dependence of the real part of the complex permittivity (ε') for the composite sheets including nanocrystalline FeCuNbSiB alloy flakes milled for 0, 12, and 24 h, respectively

Materials based on carbon nanotubes and their applications from exposure to electromagnetic fields

Here generated poly (methyl methacrylate) (PMMA) and Epoxy composites coating containing multi-walled carbon nanotubes (MWCNTs) by mechanical grinding in a planetary ball mill. The efficiency of the material's electromagnetic absorption, electromagnetic interference shielding, and reflection characteristics were presented. PMMA/MWCNTs coatings and Epoxy/MWCNTs composites exhibited complete electromagnetic radiation shielding against more than 99 percent of electromagnetic radiation. In the 100MHz–14GHz frequency range having MWCNTs loadings over 20% by weight.[3]

Table 3. EMI SE of coated (PMMA/ 25 wt% CNTs) and uncoated samples in the 100 MHz - 14GHz frequency range

Transmitting Atenna	Receiving Atenna	Frequency (MHz)	No sample (dB)	Uncoated samples (dB)	Coated samples (dB)	Shielding effectiveness (dB)
ETS 3142C	TS-EMF	100	−26.16	−27.20	−44.45	17.25
		200	−45.86	−47.29	−67.13	19.84
		300	−54.49	−57.60	−79.66	20.06
		400	−42.14	−41.15	−59.71	18.66
		500	−39.03	−39.32	−59.42	20.10
		600	−33.70	−33.87	−54.69	20.82
		700	−27.08	−26.86	−47.23	20.37
		800	−20.70	−20.64	−41.87	21.23
		900	−21.04	−20.87	−39.87	19.70
		1000	−24.72	−24.70	−44.71	20.01
		1200	−23.95	−24.04	−45.90	21.86
		1400	−30.77	−30.69	−53.01	22.32
		1600	−27.91	−28.13	−48.26	20.13
		1800	−32.91	−33.47	−54.64	21.17
		2000	−35.86	−36.73	−56.21	19.48
ETS 3115 (X-band)	HL-050	4000	−41.75	−42.34	−60.70	18.36
		6000	−51.24	−52.14	−79.76	17.52
		7000	−55.68	−57.41	−78.35	20.94
		8000	−92.19	−95.34	−114.41	19.07
		10000	−83.64	−86.20	−106.06	19.86
		11000	−86.35	−87.77	−106.72	18.95
		12000	−81.23	−84.94	−107.67	22.73
		14000	−94.35	−97.18	−116.61	19.43

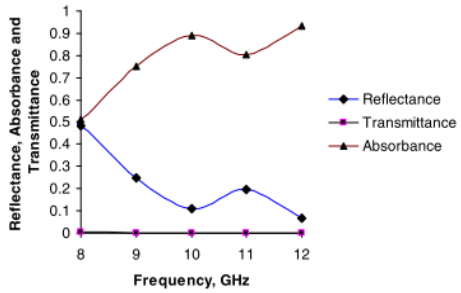

Figure 12. Reflectance, absorbance, and transmittance of PMMA/CNTs coating

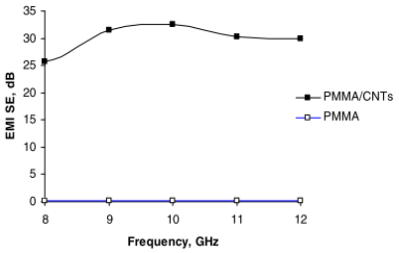

Figure 13. EMI SE of coating PMMA/CNTs at frequency 4-12 GHz

To attain the shielding of the EM threshold, a material's electrical conductivity /composites must be at least 10 Sm^{-1}, with a minimum of 25% MWCNTs filler. Meantime, the Electromagnetic interference SE of composite MWCNTs/epoxy materials exceeded 20 dB in the X–band (8–12 GHz). The reflectance of 25% The dielectric constant of the filled PMMA coating-MWCNT is roughly 0.3, and its absorbance is approximately 0.7, suggesting that the coating can block more than 99.9 percent of electromagnetic wave energy.[3]

Electromagnetic wave-absorbing composites using a conducting polymer layer with a square design

In military applications, EMWAs can lower the Radar Cross Section (RCS) of buildings, reducing the probability of radar detection. Here we talk about EMWA composite structural designs with a square periodical-shaped layer. Multi-resonance wideband absorption in composite materials may be achieved by controlling pattern shape and surface resistance.[18]

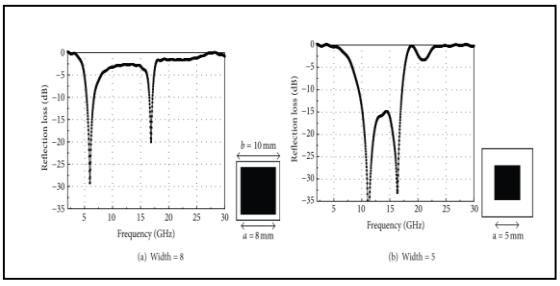

Figure 14. Peak control AMC absorber with Salisbury absorber

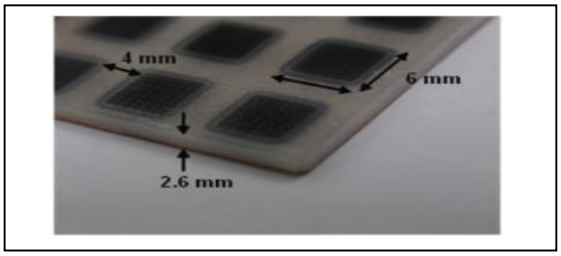

Figure 15. PPRAS composite

Figure 14 displays the AMC peak position and migration with changing square size. The first graph has a huge square and a large capacitance. AMC peak is at 6GHz and Salisbury peak is around 17GHz. The second graph has smaller squares. The AMC peak shifted right, however; the Salisbury point remained stationary. Due to this, the AMC with Salisbury peaks are blended. The multilayered RAS's thickness was controlled to provide this dual-peak control. This adjustment expands the bandwidth of absorption of EM waves in a single-layered PPRAS. [18], [19]

Radar Absorbing Structures Patterns (RAS). It acts as an electromagnetic wave reflector and shield. DC can always be conducted when the conductive surface is carved, however, AC has a particular zone at which EM waves might not be reflected or transferred. Periodic patterns, like frequencies preferential surfaces, constitute as EM wave filters.[18]

Carbon micro coil-polyurethane composite

In such a thermochemical deposition of vapor, method, CMCs were formed on Al_2O_3 materials utilizing SF_6 as an additive gas and C_2H_2/H_2 as source gases. Composites of CMCs and polyurethane made by CMCs are dispersed in PU employing dimethylformamide. CMC-PU composites were tested for electromagnetic wave shielding from 0.25–1.5 GHzCMCs-PU Shielding effectiveness increases with CMC concentration as well as layer thickness. Based on these observations, the principal SE function was discussed.[19]

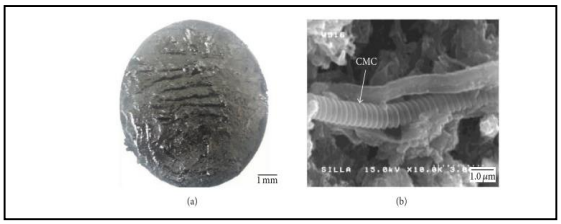

Figure 16. (a) The representative photograph of the coated layer surface on the glass plate and (b) the cross-sectional FESEM image of the coated layer showing the existence of CMCs within the PU-CMC composite

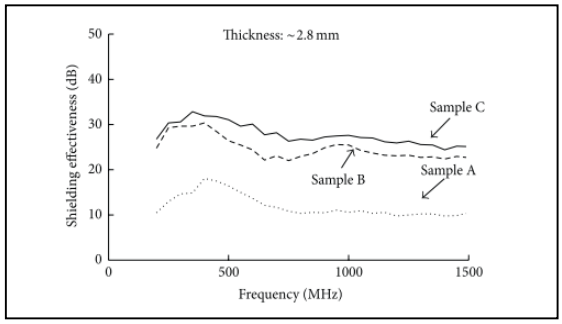

Figure 17. The variation is in shielding effectiveness relative to the different composition ratios of the CMCs in the CMC-PU-DMF mixture.

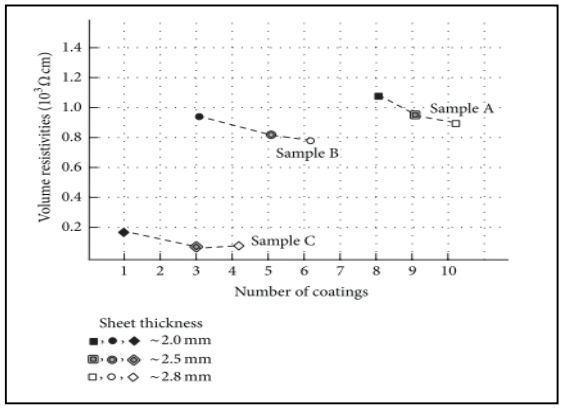

Figure 18. The dependence of the PU-CMC sheet volume resistivity relative to the number of coatings.

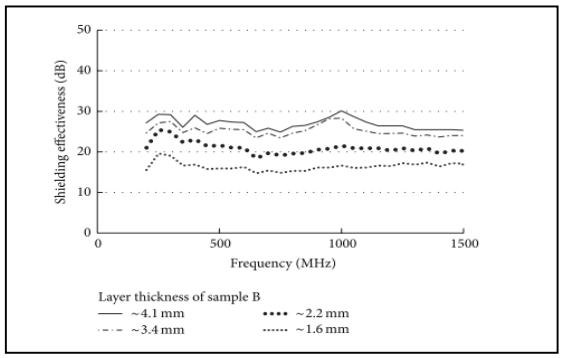

Figure 19. The variation of shielding effectiveness for sample B relative to the different thicknesses of the coated layers.

Figures 17 and 18 illustrate that the SE does not directly correlate with the volume resistivity. As a result, other than reflection, the absorption effect will be a major SE mechanism for these composites' EMI. We couldn't find a frequency dependency of the SE for these composites. Furthermore, we are certain that the standard error did not reduce as the observation frequency increased from 1.0GHz to 1.5GHz. This study also shows that reflection is not the predominant EMI mechanism in these composites. Figure 8 also shows that the SE increases with coating thickness demonstrating that the process of absorption is the primary EMI mechanism of the composite material.[19]

These PU-CMC composites had the greatest electrical conductivity and SE across samples with comparable coating layer thicknesses, Moreover, there is no precise correlation between SE and volume resistivity. The SE did not diminish when the frequency of testing increased from 1 GHz to 1.5 GHz. The SE also rises as composite layer thickness increases.[19]

Effect of magnetite nanoparticles and carbon nanofibers on electromagnetic absorption in composites.

Here epoxy composites contain varying proportions of carbon nanofibers, magnetite nanoparticles, and magnetite-decorated CNF. Adsorbing premade The attachment of oleic acid-capped-magnetite nanomaterials to the CNF surface is a straightforward way for magnetite CNF decorating. In the produced materials, the synergy between magnetite nanoparticles and CNF was revealed to be significant. Their electrical conductivity and complicated permittivity at high frequencies have been used to analyze this phenomenon. We investigated each of the electromagnetic shielding techniques from 1–18 GHz. Electromagnetic shielding effectiveness can be increased by up to 20 dB by coating CNF with magnetite. A new dissipation process called interfacial polarization might be accountable for the observed increase in EM radiation shielding.[20] EMI shielding efficiency equations are below.[21]

$$SE_T = 20\log\left(\frac{\eta_0}{4\eta_s}\right) + 20\log\left(exp\left(\frac{2d}{\delta}\right)\right) + 20\log\left(1 - exp\left(\frac{2d}{\delta}\right)\right) \quad (8)$$

$$SE_T = SE_R + SE_A = \left(39.5 + \frac{10log\sigma}{2\pi f\mu}\right) + \left(8.7d\sqrt{\pi f\mu\sigma}\right) \quad (9)$$

$$SE_T = 10\log\frac{P_I}{P_T} = 10\log\frac{1}{|S_{21}|^2}$$

$$SE_R = 10\log\frac{P_I}{P_I - P_R} = 10\log\frac{1}{1 - |S_{11}|^2}$$

$$SE_A = 10\log\frac{P_I - P_R}{P_T} = 10\log\frac{1 - |S_{11}|^2}{|S_{21}|^2} \quad (10)$$

The period of reflection depends on (r/l) but not on sample thickness, whereas the term for absorption depends on (r/l) and sample thickness. The scattering variables S_{11} and S_{21} can be measured the means of a vector network analyzer to determine their contributions to shielding (ENA). When a substance is irradiated with a P_I, an ENA device measures the P_T and P_R. The equations give the scattering parameter to transmission, reflection, and absorption SE ratios. [21]

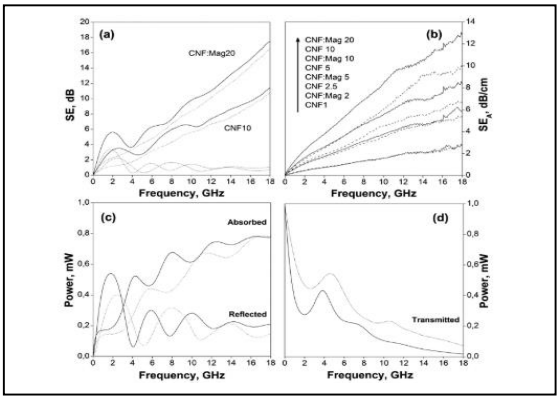

Figure 20. (a) Total electromagnetic shielding efficiency, SET, for composites CNF10 and CNF: Mag20. Reflection shielding, SER (Dot), absorption shielding, SEA (Dash), transmission shielding, SET (line). The thickness of specimens: 13 mm. (b) Absorption coefficients for CNF (dashes), CNF: Mag (lines) composites with compositions indicated in the inset. (c) Absorbed, reflected and (d) transmitted power of CNF10 (dash) and CNF: Mag20 (line)

The scattering parameters has been used to calculate SE contributions Shielding efficiency (SET) for growing CNF concentrations in both the CNF: Mag20 and CNF10 systems. Above 3–4 GHz, absorption (SEA) dominates SE, while reflection (SER) stays modest. The absorbance effect rises with frequency, attaining Mag 20 and 12 dB for CNF and 18 dB for CNF: by itself. In the reflection element, several maxima typical of reflectors from the second plane of the sample were found, which were less dependent on sample thickness and composition.[20]

Conducting polymer composite with barium ferrite nanoparticles

Through emulsion polymerization, conducting polymer nanocomposites comprising polyphenylamine and barium ferrite nanoparticles (50–70 nm) have been presented. The composite's complicated permittivity, permeability, and microwave absorption characteristics were presented in the frequency range of 12.4–18 GHz (Ku band). The composite exhibits a high shielding efficacy due to an absorption coefficient (SEA) of 28.9 dB (99.9 percent), which is highly dependent on the dielectric loss, magnetic permeability, and volume fraction of barium ferrite nanoparticles. The high SEA value indicates that these composites have potential as radar absorption materials. [22]

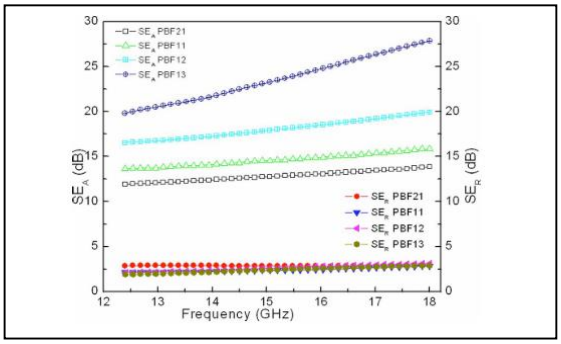

Figure 21. (Color online) Variation in the EMI shielding effectiveness, SEA, and SER of polyaniline composites having different weight ratios of barium ferrite: PBF21, PBF11, PBF12, and PBF13, with frequency

The SE change with frequency in the 12.4–18 GHz band is seen in Figure 2. SE shielding efficiency of PBF is mostly due to absorption. It is discovered that it increases with the concentration of ferrite and stabilizes after threshold loading.

The microwave absorption property of the composites is highly dependent on the intrinsic features of the hexagonal ferrite nanoparticles embedded in the polymer matrix. The composite's AC conductivity and permeability rise as the ferrite concentration increases, resulting in increased microwave absorption. The composite with a monomer-to-ferrite weight ratio of 1:3 has a SEA value of 28.9 dB -99.9 percent. The relationship between SEA and magnetic permeability and AC conductivity demonstrates that materials with greater conductivity and magnetization absorb more light.[23]

Fe_3O_4@SiO_2 core-shell polyaniline composites

Mechanical and chemical procedures can be used to successfully create Fe_3O_4@SiO_2 core-shell/polyaniline composites. The results suggest that composites containing 4% Fe_3O_4@SiO_2 core-shell filler might be used as an X-band electromagnetic absorbent material. Between 8.0 and 12.2 GHz, the frequency bands with a reflection loss of less than 10 dB (90 percent microwave absorption) are obtained at a thickness of 2 to 5 mm. This improvement might be attributable to the insertion of a filler of the Fe_3O_4@Score-shell.[24]

Fabrication of Fe_3O_4@SiO_2 core-shell polyaniline composites The oxidation process use to create Fe_3O_4@SiO_2 polyaniline-based composites. [25]

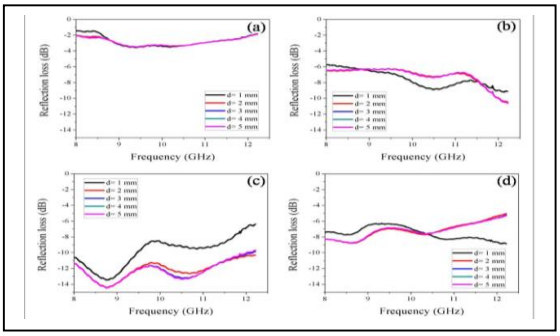

Figure 22. The reflection loss values of the Fe_3O_4@SiO_2core–shell polyaniline-based composites with various sample thicknesses and (a) 0 wt%, (b) 2 wt%, (c) 4 wt%, (d) 6 wt%Fe3O4@SiO2 core-shell fillers.

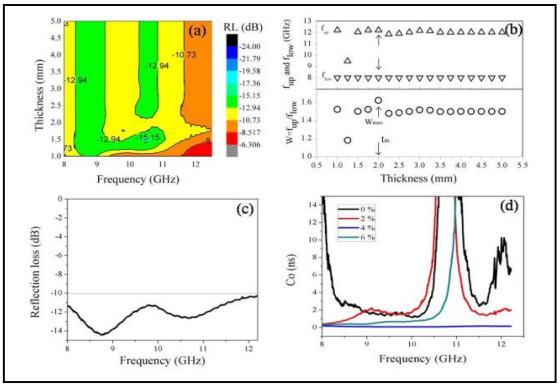

Figure 23. The Fe3O4@SiO2 core-shell polyaniline-based composites. (a) The 2D map color filling patterns of RL characteristics with various sample thicknesses, (b) the dependence off up, $f_{low,}$ and $W=f_{up}/f_{low}$ on thickness t, and (c) reflection characteristics at the optimum thickness tm for 4 wt% Fe3O4@SiO2 core-shell fillers. (d) Eddy current loss (Co) curve of 0 wt%, 2 wt%, 4 wt%, 6 wt% Fe3O4@SiO2 core-shell fillers

Table 4. Microwave absorption characteristics of some previously studied typical Fe3O4@SiO2 core-shell fillers

Composition	Minimum RL value (dB)	Optimum thickness (mm)	Optimum frequency (GHz)	Effective bandwidth (RL <–10 dB) (GHz)
Fe_3O_4/C/paraffin composites	–18.73	2.5	15.37	**5.4**
Fe_3O_4/SiO_2/graphene composite	–27.1	1.5	12.2	**2.3**
Fe_3O_4@SiO_2 microspheres	–17.55	4.5	13.7	**1.6**
Fe_3O_4@SiO_2@ZnO microspheres	–18.89	1.5	13.5	**2.5**
Fe_3O_4/PANI core/shell microspheres	–32.5	2	15.6	**5**
Fe_3O_4@SiO_2 core–shell polyaniline	**–14.42**	**2**	**8.74**	**4.2**

Microwave absorption

The reflection loss (RL) values of Fe_3O_4@SiO_2 core-shell polyaniline-based composites has been computed using equations complex permeability ($\mu=\mu'-j\mu''$) and permittivity ($\varepsilon=\varepsilon'-j\varepsilon''$). Figure 5(a) shows the RL values for various sample thicknesses on absorption characteristics for composite materials in the X band frequency range (d). This is done using various sample thicknesses from 1.0 to 5.0mm. There is an optimal outcome for each thickness of Fe_3O_4@SiO_2 polyaniline-based composites with 4 wt% (figure 5c) and 6 wt% (figure 5d). The ideal sample had a minimum RL of 14.42 dB (over 95 percent absorption) at 8.74 GHz and a bandwidth of less than 10 dB (over 90 percent absorption) at 4.2 GHz.[24]

Recent developments of smart electromagnetic absorbers-based polymer-composites

The combining of polymers and nanoparticles allows for the integration of inorganic materials' high electric/magnetic losses and the polymer's ease of tenability. It may be the ideal technique for designing effective EM wave absorption materials.

Table 5. Typical applications of ferrite absorbers

Example of absorber	Type of absorber
Anechoic chamber	Two-layer absorber consisting of carbon and ferrites. Ferrite single-layered absorber—multilayered absorber consisting of resistive film and ferrite (flooring in anechoic chamber).
The wall panel of the building (countermeasure for TV ghosting)	The absorber consists of a concrete (stone) panel and a ferrite plate. Counter absorber containing ferrite particles
Countermeasure for suppressing unnecessary echo in ship's radar signals	Single rubber ferrite absorber Absorber of thick paint plate. Two layered absorbers consisting of metallic fiber and rubber ferrite.
Countermeasure for leakage wave from electric devices	Rubber ferrite absorber Plastic ferrite absorber

When a substance is a perfect conductor, it has no skin depth. At microwave frequencies (10 GHz), the skin depth of a good conductor such as copper is around 0.65 μm. As a result, the lower the microwave electrical conductivity, the greater the electromagnetic field's capacity to propagate through the material. The depth of the skin is dependent on the frequency of the applied wave, and it changes with frequency. Thus, the following equation may be used to determine the frequency, electrical conductivity, magnetic permeability, and skin depth.[26]

$$\delta = \frac{1}{\sqrt{\pi f \mu_0 \mu_r \sigma}} \qquad (11)$$

The following equation may be used to illustrate the connection between thickness, permeability, and frequency of minimal reflection loss:

$$f_m = \frac{c}{2\pi\mu'' d} \qquad (12)$$

f_m: matching frequency with minimum reflection loss
μ": imaginary permeability
c: velocity of light
d: sample thickness

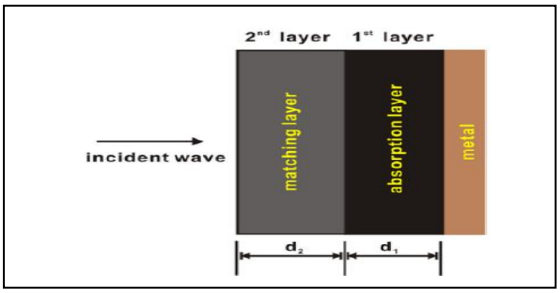

Figure 24. Structure of proposed double-layer microwave absorbing material layers,

To meet the demand for a broad absorption bandwidth, several research studies have been conducted using multilayers as seen in Fig 24.

Table 6. Relationship between reflectivity reduction and the absorbed energy

Reflective reduction(dB)	Absorbed energy %
0	0
-3	50
-10	90
-15	96.9
-20	99
-30	99.9
-40	99.99

FILLERS

The type of filler used in a polymer matrix is critical for achieving optimal and increased absorption. By integrating dielectric and magnetic fillers, these materials' electromagnetic characteristics may be enhanced, resulting in maximal electromagnetic energy absorption.

Choosing materials with high absorption across a wide frequency range might solve difficulties (combination of particles with both magnetic and dielectric loss). Adding a dielectric and magnetic filler to a polymer matrix also improves microwave absorption. To absorb many frequencies, many researchers combine magnetic (soft or strong magnet) and dielectric absorbers. A material with a combination of grain sizes can also achieve a wide range of absorption. It refers to the idea of having various anisotropy fields as grain size increases. This causes broad-band absorption. The most critical stage in developing a broadband absorber is to carefully characterize the frequency response of the constituent material characteristics.[26]

polyaniline nanofiber-based functional absorbers

In situ, polymerization of polyaniline nanofibers and graphite composites on cotton and nylon textiles produced flexible and lightweight EMI shields. The polyaniline nanofiber graphite composite can be made by polymerizing graphite flakes with a 4:1 aniline monomer–filler ratio. The polyaniline nanofiber graphite composite proved good EMI shielding in the range of 83–89 dB for a wide frequency range of 8.2–18 GHz when the conducting filler is added. Absorption is the main shield of polyaniline nanofibers and the polyaniline nanofiber graphite composite-based advanced textiles are thin (0.1 mm) and demonstrated EMI shielding of 15 dB for polyaniline nanofiber graphite composite-based fabrics. Thus, flexible, thin, broadband shielding materials that can block roughly 97 percent of EMI have been produced. These polyaniline nanofiber-based textiles can address the rising demand for thin and flexible EMI shielding materials. [27],[28]

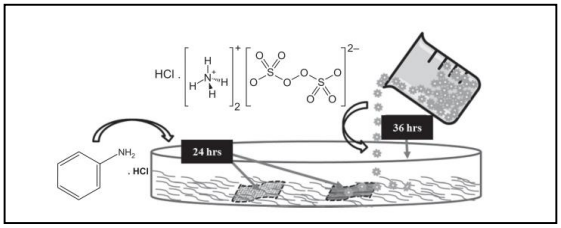

Figure 25. Schematic representation of the preparation of functional cotton and nylon fabrics based on polyaniline nanofibers and their composite.

Figure 26. Transmission electron microscope of (a)graphite, (b)

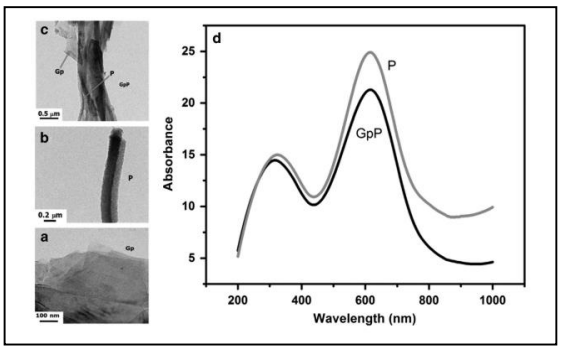

polyaniline nanofibers (P) and (c) polyaniline nanofiber graphite composite (GpP), and (d) solid-state ultraviolet-visible spectra of polyaniline nanofibers and their graphite composite.

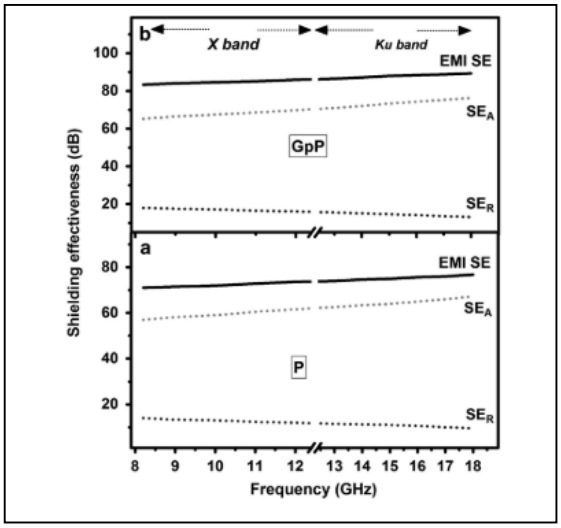

Figure 27. Variation of EMI SE, SE_A, and SE_R of (a) polyaniline nanofibers (P) and (b) polyaniline nanofiber graphite composite (GpP) of thickness 1 mm in the 8.2–18 GHz frequency range.

Polymer Composites of W-Type Hexaferrite Powders by Attachment of Frequency Selective Surface

The influence of a frequency selective surface (FSS) made up of square loop(SL) components on the absorption characteristics of grounded ferrite composites is presented. Substrates were polymer matrix composites of CoZnW hexaferrite powders with low magnetic loss. The reflection coefficient was computed by modeling the interaction of electromagnetic waves with materials. Attaching an FSS with regulated electrical resistance (R) to the grounded ferrite composites enhanced reflection loss and bandwidth. The FSS with R = 800Ω has a minimum reflection loss of –25 dB at 10 GHz and a bandwidth of 7.5-12.5 GHz at –10 dB.[29]

It is investigated here how an FSS made up of square loops affects the absorption characteristics of grounded ferrite composites. Substrates were polymer matrix composites of CoZnW hexaferrite powders with low magnetic loss.

Computational methods (HFSS 13.0) has been utilized to study electromagnetic wave-material interaction.

The absorber structure consists of a ferrite composite substrate has been separated by a square loop FSS (SL-FSS) on the top layer and a perfect electric conductor (PEC) on the bottom layer.[29]

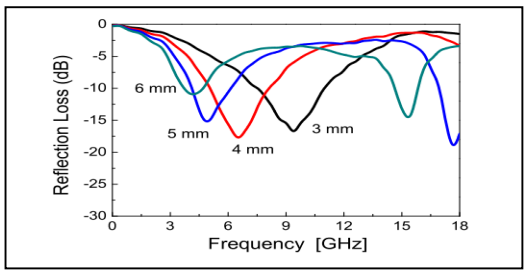

Figure 28. Reflection loss determined in the grounded ferrite composites with various layer thicknesses

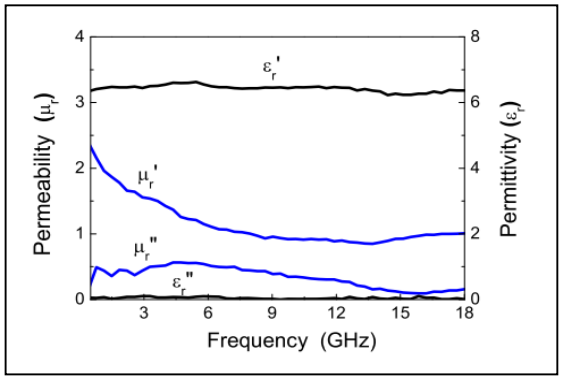

Figure 29. Complex permeability and permittivity of rubber composite containing CoZnW hexaferrite powders

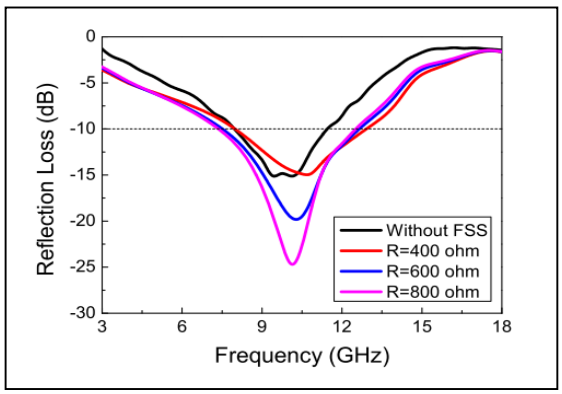

Figure 30. Reflection loss was determined in the composite structure, implemented with SL-FSS on a grounded ferrite composite (thickness = 2.9 mm), with increasing SL-FSS resistance (R)

Fig. 29 complex permeability (μr = μr' – jμr") and The hexaferrite powders in CoZnW rubber composites have permittivity. (Fig.30) PEC grounded ferrite composite with varied layer thicknesses is shown in Figure 30. The absorption frequency spectrum narrows with layer thickness.[30]

Carbonyl iron/MnZn Ferrite/PVC polymer composites[31]

The electromagnetic wave absorption properties of CI/MnZn/PVC composites were presented in the frequency range of 10 MHz to 6.5 GHz. Rising permeability and magnetic resonance loss (particularly in the GHz frequency region) due to increased carbonyl iron loading reduces matching thickness and shifts the absorption peak towards a lower frequency. Increasing MnZn ferrite loading (and decreasing carbonyl iron) increases absorption bandwidth. The results show that the flexible composites may act as thin or wideband microwave absorbers.[32]

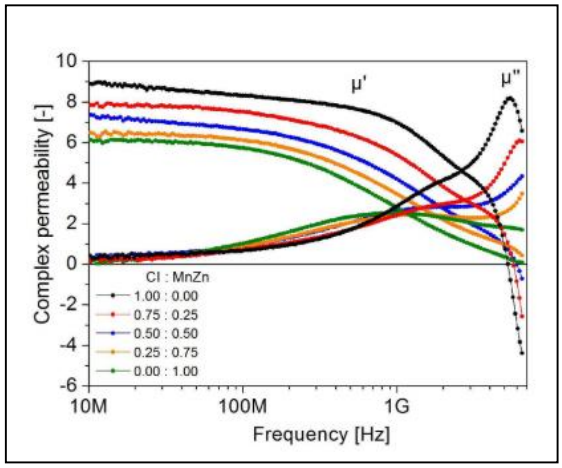

Figure 31. Frequency dependences of real and imaginary parts of complex (relative) permeability for prepared CI/MnZn/PVC composites with different filler volume ratios.

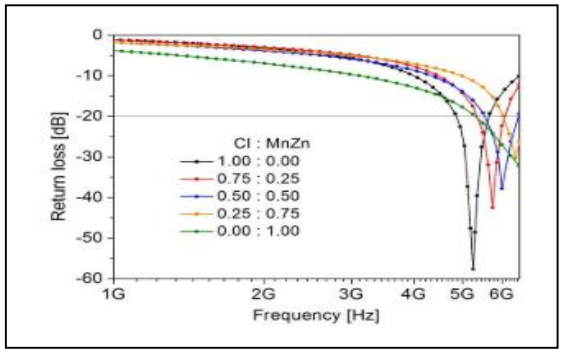

Figure 32. Frequency dependences of return loss for prepared CI/MnZn/PVC composites with different filler volume ratios.

Polymer-based composites have low density and can link fillers, making them ideal for shielding purposes. PVC polymer is used as the matrix because it is flexible and has good chemical and electrical characteristics.

Table 7. Absorption parameters for fabricated CI/MnZn/PVC composites of different filler volume ratio CI: MnZn

Ratio	*dm* [mm]	*fm* [GHz]	Δ*f* [MHz] (RL≤ −20 dB)	RL*min* [dB]
1.00:0.00	1.38	5.25	690	−57.61
0.75:0.25	1.44	5.74	750	−42.43
0.50:0.50	1.96	5.99	970	−37.80
0.25:0.75	2.08	6.39	> 1000	−30.28
0.00:1.00	4.32	6.50	> 1000	—

The absorption characteristics of metal/ferrite/polymer composites containing carbonyl iron and manganese-zinc ferrite as two-phase fillers and polyvinylchloride as matrix were presented in detail (10 MHz–6.5 GHz). The results demonstrated that the return loss and complicated permeability of composites had a considerable impact on high-frequency absorption capabilities. With increased carbonyl iron volume loading, the absorption peak migrated to a low frequency and the matching thickness dropped. However, the absorption bandwidth rises with MnZn ferrite filler content. The researched composite materials allow for thin, flexible microwave absorbers.[32]

Nanosized conducting black-silicone rubber composites

This research reports on broadband microwave absorption and electromagnetic shielding performance in flexible rubber composites with low nanosized conducting carbon filler concentration throughout the 8–18 GHz frequency range. In a silicone rubber matrix, 1–15wt% nanosized conducting Carbon Black (CB) has added. The effect of nanosized CB loading on DC conductivity, dielectric and microwave absorption characteristics, and SE of silicone rubber composites is presented. The percolation threshold has reached at a 3wt% CB content in composites. A composite with a 5wt% CB concentration may offer over 90% microwave absorption (Reflection Loss >-10 dB) over 8–18 GHz at a composite thickness of 1.9–2.7mm. Moreover, at 2.8mm thickness, composites containing 15% CB demonstrate 40 dB SE throughout the frequency range of 8–18 GHz. The article present the impact of composite thickness on microwave absorption and shielding. They can be employed as microwave absorbers in stealth applications and for EMI shielding of electronic equipment in many civilian and military fields. [33],[34],[35]

The reflection loss (RL) of composites as microwave absorbers has determined using complicated relative permittivity (ε) and relative permeability (μ). The normalized input impedance (Zn), reflection coefficient (Γ), and RL (in dB) of a PEC supported single layer absorber are described as follows:[33]

$$Z_n = \frac{Z_m}{Z_0} = \sqrt{\frac{\mu}{\varepsilon}} \tanh\left[j\left(\frac{2\pi f d}{c}\right)\sqrt{\mu\epsilon}\right]$$

$$\Gamma = \frac{Z_n - 1}{Z_n + 1}$$

$$\text{R. L.} = 20\log_{10}|\Gamma| \qquad (13)$$

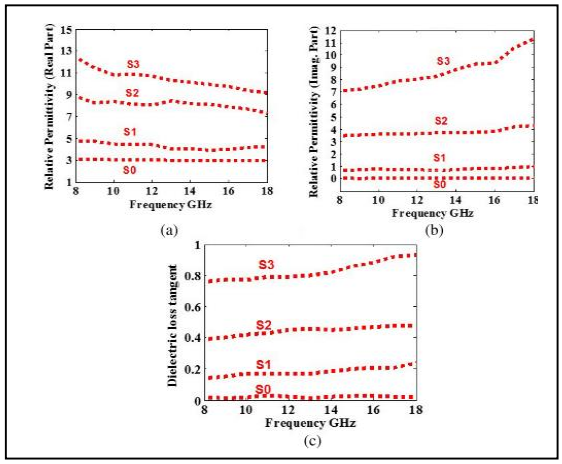

Figure 33. Complex permittivity vs. frequency. (a) Real part (ε'). (b) Imaginary part (ε''). (c) Dielectric loss tangent (tan δ $_{\varepsilon}$)

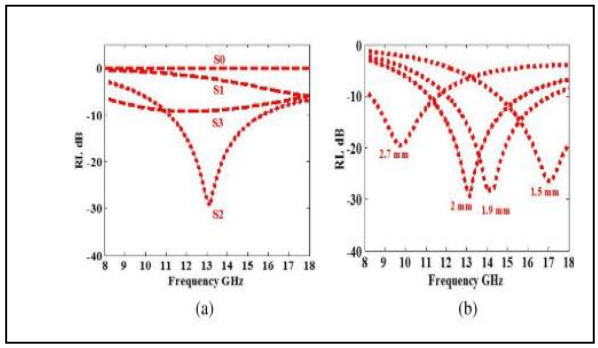

Figure 34. Reflection loss (RL) vs. frequency (a) RL of samples S_0–S_3 at thickness 2mm (b) RL of sample S_2 at different thicknesses. S1, S2, S3 and S4 are samples made with 3wt%, 5wt%, 10wt%, and 15% nanosize carbon.

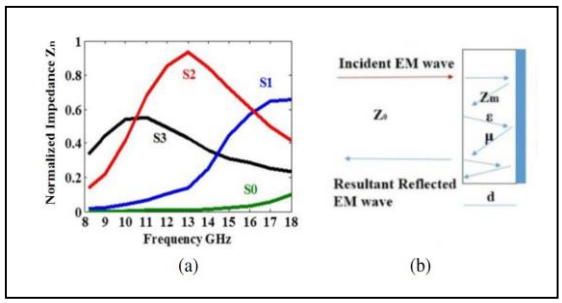

Figure 35. (a) Normalized impedance vs. frequency of all samples at thickness 2mm. (b) Schematic of RL phenomenon of a single layer MW absorber.

Graphene oxide reinforced epoxy resin polymer as a composite

The ammonia solution approach has been used to make rGO. Using a mini-mechanical vortex mixer, the study present the effect of cured epoxy composites containing rGO. The effect of rGO powder and loading on dielectric and mechanical characteristics was compared. The samples has been characterized using FT-IR, XRD, and FE-SEM. On 8-12 GHz, the rGO/cured epoxy composite dielectric characteristics results were analysed. Even at 1% concentration, rGO in the cured epoxy matrix exhibits modest dielectric characteristics. The suppressive shielding efficacy of the composite with 5 percent rGO in the cured epoxy matrix is 25.748 dB at 12 GHz and 6 mm thickness. Cole-ColeCole plots revealed just one dielectric relaxation process for rGO/cured epoxy composites with low impedance match characteristics due to inadequate microwave absorption. Its groups and residual defects can increase the impedance match characteristics, as well as polarization relaxation of electronic dipole groups and defect polarization relaxation, which all favor electromagnetic wave absorption and penetration.[4]

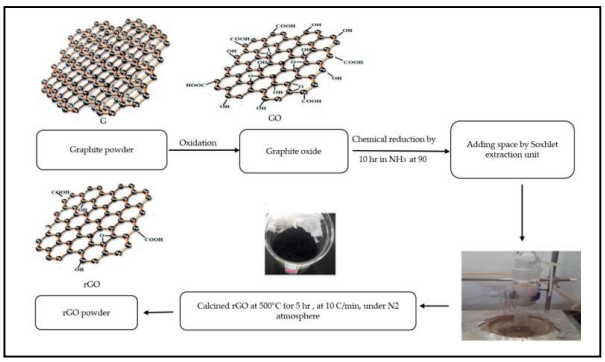

Figure 36. Schematic drawings for the preparation of reduced graphene oxide paper and powder by using the spaced method in a soxhlet unit. GO, Graphite Oxide; rGO reduced GO.

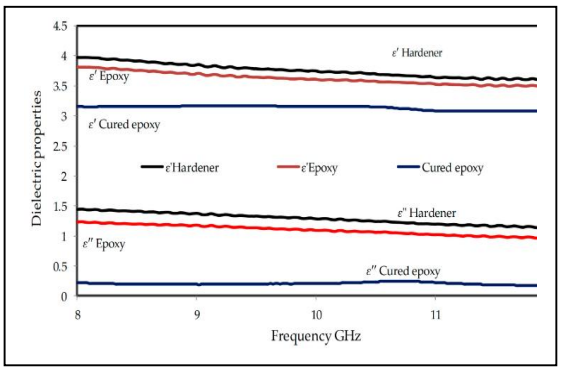

Figure 37. Relative permittivity for the epoxy, the hardener, and the cured epoxy at the X-band frequency

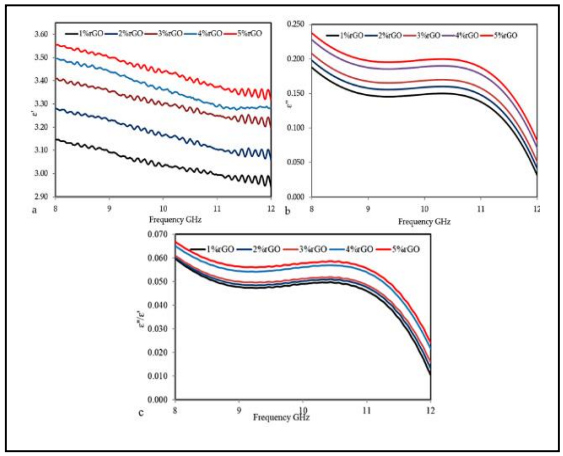

Figure 38. The frequency dependence of (a) The real part of permittivity (ε'), (b) The imaginary part of permittivity (ε"), and (c) The tangent loss (tanδ) at various rGO loadings.

Table 8. The SE $_{total}$ (dB) values for the rGO composites dependent on the frequencies and percentages of filler

Freq (GHz)	1 wt %	2 wt %	3 wt %	4 wt %	5 wt %
8	5.233	5.061	4.912	4.451	4.927
9	7.309	7.322	7.038	7.239	7.476
10	9.516	9.556	9.872	10.109	10.692
11	12.038	13.226	13.779	14.444	15.991
12	16.046	19.434	20.226	21.933	25.748

Novel green composites of coconut fiber coir and charcoal powder

This research discusses the EW absorption properties of innovative green composites made of coconut fiber coir and charcoal powder. For the samples, coir, charcoal powder, epoxy resin, and hardeners of varying compositions. The materials' dielectric characteristics have been measured using a two-port waveguide spanning the X-band (8.2–12.4GHz). The average permittivity is around 3.00, with 10% charcoal having the highest at 3.59. Besides that, all samples had good reflection loss of more than -25dB, indicating over 99 percent absorption. Thus, composite materials are potential organic materials for EM absorber applications.[13]

Table 9. Average dielectric constant and reflection loss of some material

Material	Dielectric constant	Reflection loss
Coco-peat	>3.0	<-30dB
Rice husk and carbon nanotubes	>3.0	<-20dB
Coconut fiber coir and charcoal	>3.0	<-25dB

Table 10. The average of absorption properties over the x-band frequency

Sample	ε'	μ'	σ	d_p	α	β	RL
Coir	3.4566	1.2617	0.1931	0.0282	21.6581	451.5935	-28.0460
5wt% Charcoal	3.5246	1.2919	0.1245	0.0891	13.7791	460.4311	-28.3375
10wt% Charcoal	3.5905	1.2173	0.1354	0.0398	14.7316	451.4801	-26.7260
15wt% Charcoal	2.9948	1.1620	0.1164	0.0397	13.6474	402.9805	-29.2444
Charcoal	3.1781	1.2152	0.0719	0.0674	8.3511	423.7698	-29.0561

Polyvinylpyrrolidone-TiO_2/polyacrylonitrile-SiO_2 nanofiber nanocomposites

The SE and UV shielding performance of PVP–TiO_2/PAN–SiO_2 nanofiber nanocomposites generated by single nozzle co-electrospinning are reported here. Three samples with varying average diameters have beeen electro-spun at 0.3, 0.4-, and 0.5-ml h^{-1}. The core-shell structure of nanofiber nanocomposites has been validated morphologically. The EMI SE of the nanofiber nanocomposites has investigated at room temperature using a vector network analyzer. All samples exhibit good microwave absorption characteristics. An average 596.67nm diameter PVP–TiO_2/PAN–SiO_2 nanofiber shows the highest overall EMI (110dB at 9GHz) and 98 percent UV shielding.[36],[37]

One-dimensional nanofiber nanocomposites are excellent for use as an electromagnetic shield. Nanofibers are frequently utilized for microwave absorption and EMI shielding. This work has used a single nozzle co-electrospinning approach to create PVP–TiO_2/PAN–SiO_2 nanofiber nanocomposites. In the first step, a novel structure of TiO_2 and SiO_2 nanoparticle nanocomposites have been created. The performance of nanofibers with various average sizes is next explored.[36]

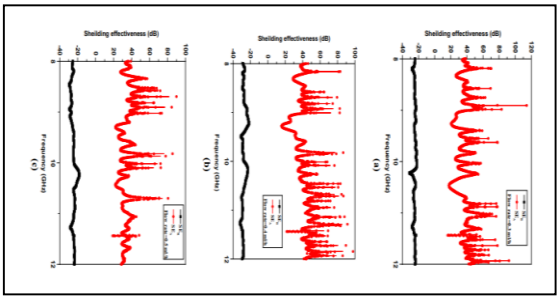

Figure 39. SE_A and SE_R of PVP–TiO_2/PAN–SiO_2 nanofiber nanocomposites that were synthesized with (a) 0.3, (b) 0.4 and (c)0.5mlh^{-1} flow rates

Table 11. Electrical conductivity of some of nanostructures

Composites	Conductivity (S cm−1)
PANI/ANF	300
Polyethylene–carbon nanofiber	10−5
MWCNTs	10−1
TS1 nanofiber	6.28

Table 12. A comparison of EMI shielding performance of various nanocomposites.

Composites	SER (dB)	SEA (dB)
Fe3O4/carbon nanofiber	11	31
MWCNFs/PPC	32.5	5
Fe3O4@SiO2@ZnO	—	25
e_3O_4@SiO_2	—	23
Flexible graphite	—	129

Polymer matrix composites as broadband radar absorption

This article summarized many researchers' efforts to construct broadband stealth composite structures utilizing various techniques. RAS can perform dual functions such as weight-bearing and radar absorption. The EM characteristics of the RAS may be adjusted by using radar-absorbing fillers, multilayered grid devices like FSS, metamaterials, CA absorbers, etc. These fillers are either particulate (powder, flakes, spherical) or fibrous in NY radar absorption fillers are carbon-based, such as CCB, carbon fibers, single-walled and MWCNTs, graphene, reduced graphene oxides, and so on. These fillers add attenuation via conduction, absorption, dielectric, and magnetic losses. These materials can be utilized directly as absorbing/reinforcing fillers in composites or as an absorbing coating on composites. The widening in multilayer grid devices occurs due to various resonances, energy redirection, etc. This gadget can widen the bandwidth in a thinned-out structure.[38]

Thus, attempts to compile viable strategies to construct lightweight thin RAS for broadbands without compromising structural integrities. The development of effective RAS for stealth aircraft requires the collaboration of aeronautical, electrical, material, and mechanical experts.

Stealth or low observable technology has been a crucial necessity for military aircraft to fight the ever-advancing target detection systems globally. One of the main dangers is Radar, which assesses the aircraft's radar cross-section (RCS). Thus, researchers are working hard to produce low RCS polymer matrix composites (PMCs) to replace highly reflecting metallic aircraft components. This review article considers the state-of-the-art advanced research on the realization of RAS using a combination of RAMs and multilayered grid devices such as frequency selective surfaces, circuit analog absorbers, metamaterials, and so on to provide superior performance RAS for stealth aircraft.[38]

These devices have recently acquired prominence because of their simplicity of manufacture, reduced thickness, and increased performance in broad bandwidths.

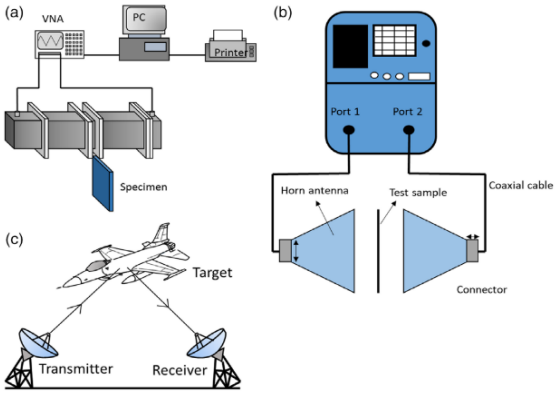

Figure 40. Test methods for electromagnetic evaluation of radar-absorbing materials. (a) Waveguide. (b) Free space. (c) Open range RCS measurements. [Color figure can be viewed at wileyonlinelibrary.com]

Table 13. Relation Between RCS and Reflection Loss

RCS reduction (%)	Reflection loss (dB)
0	0
90	10
99	20
99.9	30
99.99	40

Table 14. Material Constitution Which Resulted in more than 30 dB Loss RAMs

[22] RAMs	[23] Thickness of layer (mm)	[24] Spacer material	[25] Thickness of spacer (mm)	[26] Total thickness (mm)
[27] CN/CB4/CF2a	[28] 0.51	[29] Rohacell	[30] 1.3	[31] 1.81

Table 15. List of Dielectric/Semiconducting RAMs for Broadband Absorption RAM

RAM fillers	Type	(GHz)	loss (dB)
Carbon black and short carbon fibers	Semiconducting and conducting	8–12	27
Foliated graphite nanocomposites (FGN)	Semiconducting	1–18	37
Short carbon fiber	Conducting	8.2–12.4	7–11
Carbon black, carbon fiber, multiwalled carbon nanotubes	Semiconducting and conducting	8–18	35
Conducting carbon black	Semiconducting	8.2–12.4	55
Carbon nanotubes	Semiconducting	2–18	24.27
Carbon nanotubes, reduced graphene oxide	Magnetic, dielectric	2–18 GHz	55
Graphene	Dielectric	2–18 GHz	37.8
Reduced graphene oxide	Dielectric	2–18 GHz	10–57
Carbon, reduced graphene oxide	Dielectric	2–18 GHz	38.8
Carbon nano fibers, fullerenes, micro-sized granular graphite, Single walled and multiwalled carbon nanotubes	Semiconducting/ conducting	8.2–12.4	10
Carbon black	Conducting		22.2
Multiwalled carbon nanotubes	Semiconducting	8–12	30

Table 16. List of Magnetic and Magneto Dielectric RAMs for Broadband Absorption

Filler material	Type	Frequency (GHz)	Maximum reflection loss (dB)
M-type Hexa ferrite	Magnetic	8.2–12.4	24.5
Fe_3O_4/TiO_2	Magnetic, dielectric	5.8	
PAN coated with Ni and CO	Magnetic and dielectric	8–18	32
MnZn ferrite	Magnetic	2–18 GHz	38 dB
Fe_3O_4	Magnetic	1–18 GHz	25–30 dB
Fe3O4, RGO	Magnetic and dielectric	2–18 GHz	60–70
NiZnCo ferrites and RGO	Magnetic and dielectric	2–18 GHz	51.8
Fe, Graphene	Magnetic, dielectric	2–18 GHz	45
Ni, Graphene	Magnetic, dielectric	2–18	16
Carbonyl iron, Graphene	Semiconducting	2–18	40.2
MWCNT/ZnO / Fe_3O_4	Conducting, magnetic	2–18	40.9

Table 17. Effect on Mechanical and Physical Properties of RAS with RAM Usage

Composite system	Absorbing materials	Mechanical tests performed	Observation	Frequency
E glass epoxy and UHMWPE	Nano-sized carbon black	Low velocity impact, followed by	Tensile properties increased,	10 GHZ
as radome		compression after	compression	
		impact, tension,	decreased, other	
		compression	properties little	
			affected	
Glass epoxy	Multiwalled carbon nanotubes	Interlaminar shear strength	Presence of delamination alters RAS performance	8–12
Glass epoxy	Carbon black and CNTs	Tensile properties	3.8% hike in tensile modulus and 5.7% hike in tensile strength	8–12
Glass epoxy	Multiwalled carbon nanotubes	Tensile, Shear	Tensile strength and modulus are increasing but shearproperties decreased	12–18
Glass epoxy	Multiwalled carbon nanotubes and carbon nano fibers (CNFs)	Compression, tension,ILSS	Filler addition increases the viscosity, increase in tensile, and compression, ILSS merely affected	
Glass epoxy	MWCNT	Tensile, compression, and shear in normal, axial,and in-plane direction	Tensile strength, tensile modulus, stiffness: increases in normal mode, not improved in in-plane mode, increases in axial mode. Compressive strength and modulus decrease in normal and in-plane mode but increase in axial mode. Shear properties decrease in all modes	12–18 GHz
Polypropylene	Conducting Carbon	DMTA, hardness,	The elastic and storage	5–8 GHz
composites	black (CCB), carbon fiber (CF)	impact, tensile	modulus improved dueto modified interfaces	
			in CCB and CF PP	
			composites (DMTA).	
Epoxy composite	MWCNT	Tensile	Young's modulus and the yield strength	10–1 to 107 Hz

Table 18. Radar Absorption Using Multilayer Grid Devices

Type of multilayer grid device	**Frequency (GHz)**	*Maximum reflection loss (dB)*
FSS pattern using intrinsic conducting paste	8–12	*10 dB*
FSS structure/metamaterial	3–18	*98%–99% at 4.10, 6.15, 10.05, 15.52 GHz*
FSS	8–12	*90%*
Fractal FSS	4–12	*10 dB*
CA with conducting materials ITO and AZO	4–12	*10 dB*
Circuit analog	10	*15*
FSS	4–18	*10*
FSS with carbonyl iron flakes	4–18	*10*
Wide angle triple band metamaterials	2–12	*99% at 4.06 GHz, 93% at 6.73 GHz, and 95% at 9.22 GHz*
Uniform and non-uniform short strip pair metamaterial	8–12	*Near zero permittivity*
Resistive FSS	8–12	*90% absorption*
Split ring and multiple split ring resonators with resistive sheet	3.5–7	*97.4% and 98.4% absorption*
Electrically coupled LC resonator and split ring resonator	2.4–3	*99.9% absorption*
Metamaterial with metal spilled coin	2–8	*90%*

Polyaniline-Graphene nanoplatelet composite films

PANI – Graphene nanoplatelet (GRNP) composite films (thickness 1.5 mm) has been created by in situ polymerization of aniline in the presence of Graphene nanoplatelets. Various analytical techniques have been used to analyze the films' structural and morphological properties, including SEM, FTIR, X-ray diffraction, Raman spectroscopy, and thermogravimetric analysis (TGA). The addition of GRNPs in the PANI matrix increased the composites' conductivity and dielectric characteristics by forming 3D conducting networks. The X-band microwave shielding efficacy of PANI-GRNP composite films have doped with p-TSA then have evaluated utilizing S-parameters from a vector network analyzer. Composite shielding effectiveness is strongly correlated with GRNP concentration in the PANI matrix. When aniline diffuses into graphene nanosheets, it increases interfacial polarization due to the solid-state charge transition between PANI and GRNPs. Its shielding performance (>95%) in the X-band is outstanding with 10% GRNPs in the PANI matrix. The results show that dominating absorption contributes to total EMI SE in composites. Composites with these qualities can be used for electromagnetic shielding applications in X-band microwave frequencies.[39]

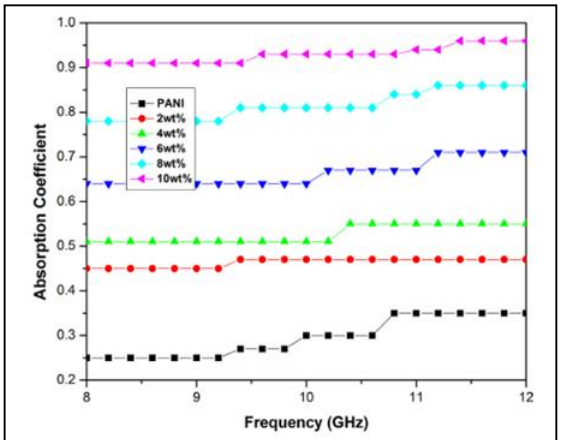

Figure 41

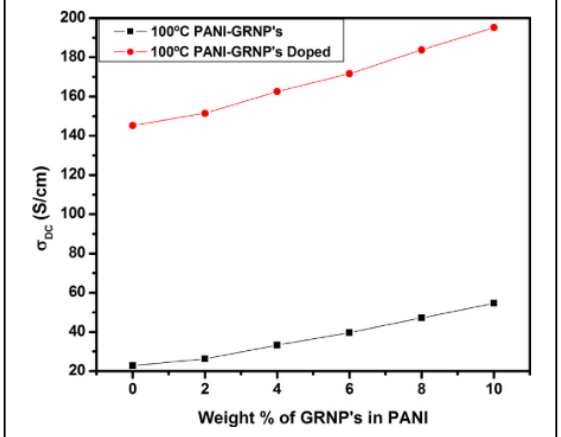

Figure 42

Figure 41. DC conductivity as a function of GRNP's content in PANI at 100 °C (PANI-GRNP's and p-TSA doped PANI-GRNP's composite). Figure 42. Absorption coefficient as a function of frequency for PANI and PANI-GRNP's composite in X-band

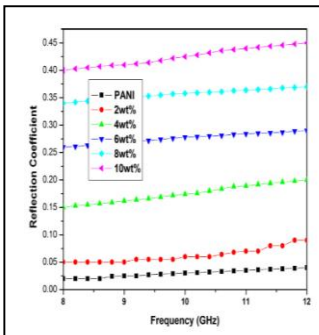

Figure 43

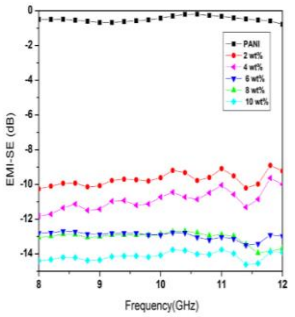

Figure 44

Figure 43. Reflection coefficient as a function of frequency for PANI and PANI- GRNP's composite in X-band. Figure 44. EMI-SE as a function of frequency for PANI and PANI-GRNP's composite in X-band

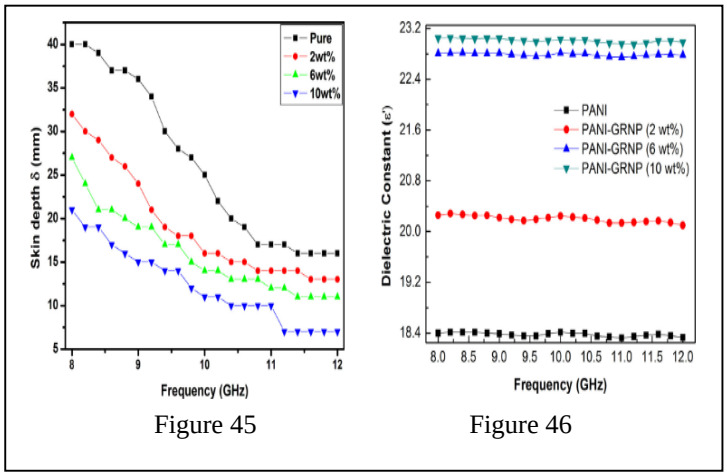

Figure 45 Figure 46

Figure 45. Skin depth as a function of frequency for PANI and PANI-GRNP's composite in X-band. Figure 46. Variation of dielectric constant as a function of frequency for PANI and PANI-GRNP's composite in X-band

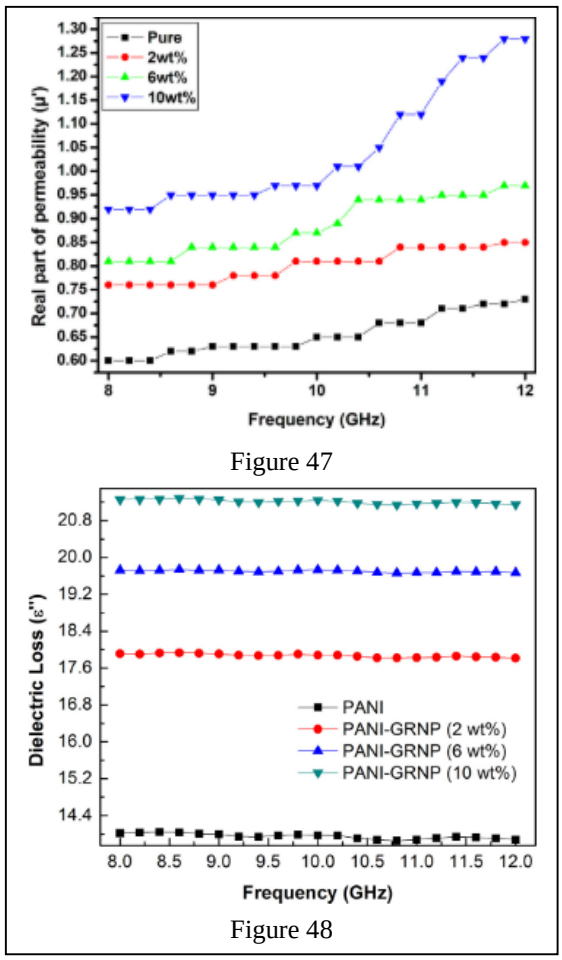

Figure 47

Figure 48

Figure 47. Variation of dielectric loss as a function of frequency for PANI and PANI-GRNP's composite in X-band. Figure 48. Variation of the real part of magnetic permeability as a function of frequency for PANI and PANI-GRNP's composite in X-band

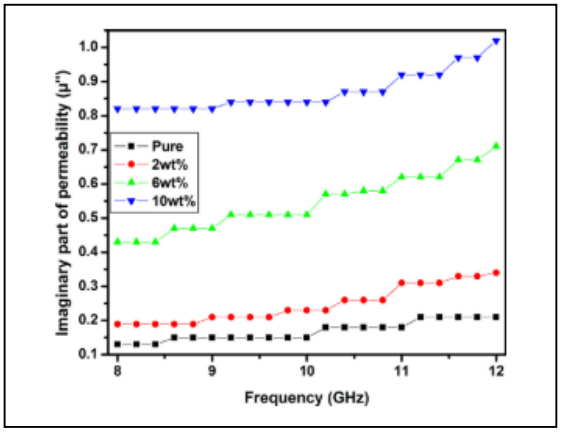

Figure 49. Variation of the imaginary part of magnetic permeability as a function of frequency for PANI and PANI-GRNP's composite in X-band

Ferrite and tantalum pentoxide based polypyrrole nanocomposite

The EMI shielding capabilities of polypyrrole/barium ferrite/tantalum pentoxide nanocomposite have been investigated in the X-band from 8.2 to 12.4 GHz. The nanocomposites have been made chemically at room temperature and subsequently analyzed. The dielectric material properties can be estimated using the Nicholson–Ross, and Weir methods. The shielding effectiveness of up to 50 dB was found to be dependent on the dielectric loss and weight fraction of ferrite and Ta_2O_5 in the polymer matrix. On the x-band frequency region, here presents the synthesis and characteristics of a polymer composite for electromagnetic interference absorption. The composite has a high permittivity polymer, a conducting polymer (polypyrrole), magnetic barium ferrite, and a dielectric (Ta_2O_5). Polypyrrole is a promising commercial conducting polymer.[40],[41]

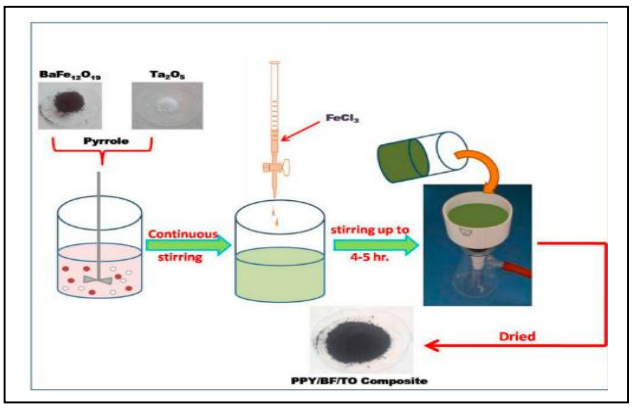

Figure 50. The schematic diagram for the synthesis of polypyrrole-barium ferrite-tantalum pentoxide (PPY/BF/TO) composite.

Table 19. Electromagnetic shielding effectiveness of different PPy based composites.

Composites	Frequency range	Shielding effectiveness (dB)
PPY-Fe_2O_3	12.4–18 GHZ	28.4
PPY	12.4–18 GHZ	7
PPY-Barium ferrite	2.0–18 GHz	11.8
PPY-TiO2	12.4–18 GHZ	13
PPY-Barium Ferrite-Tantalum pentoXide	8.2–12.4 GHz	50

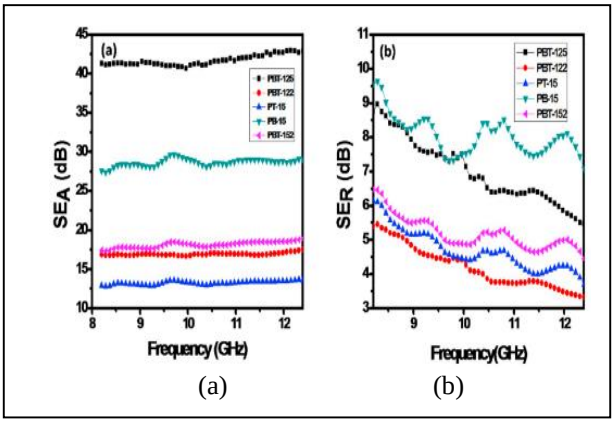

Figure 51. Variation of shielding effectiveness due to (a) absorption, (b) reflection, of polypyrrole/barium ferrite/tantalum oxide composites with frequency

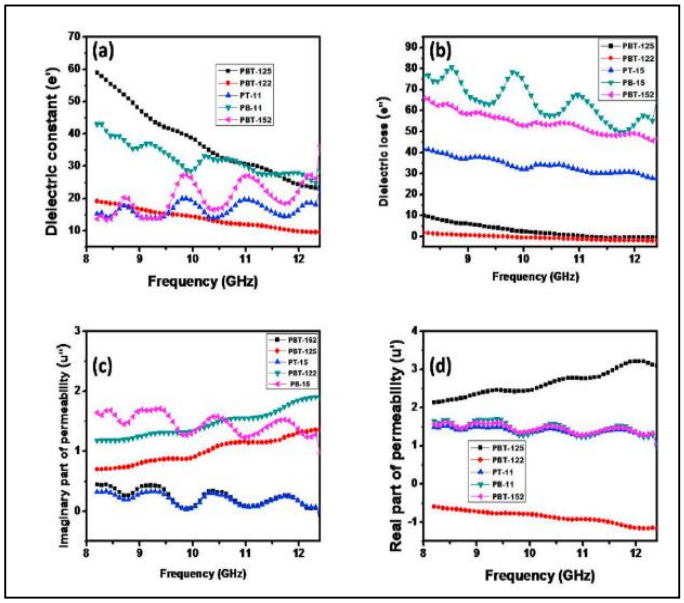

Figure 52. The behavior of (a) real (ε'), (b) imaginary (ε'') parts of complex permittivity of PPy nanocomposites as a function of frequency. (c) Dependence of real (μ′) and (d) imaginary (μ″) parts of magnetic permeability nanocomposites on frequency

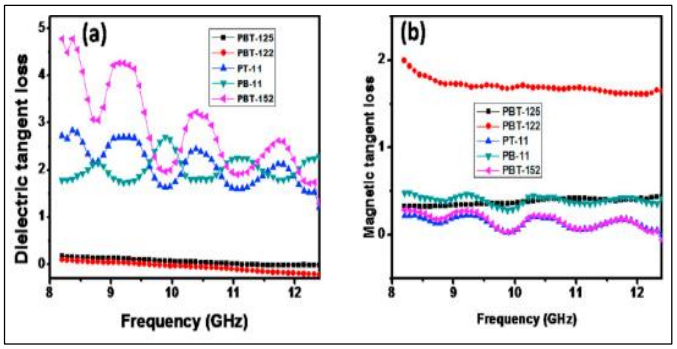

Figure 53. Variation of (a) dielectric tangent loss and (b) magnetic tangent loss with frequency

2) Status of domestic research(China)

rGO/p-Fe_3O_4@PANI three-phase nanomaterials

To provide an improved electromagnetic wave reflection interface and lengthen the reflection route of electromagnetic waves traveling inside and across materials, conductive polyaniline has been coated over reduced graphene oxide (rGO) and porous Fe_3O_4 (p-Fe_3O_4) [42]. Here presents three rGO/p-Fe_3O_4@PANI samples. PANI mass% in samples was determined. The rGO/p-Fe_3O_4 mass ratio can be modified to improve impedance matching and attenuation constant. This material is superior to rGO/p-Fe_3O_4 in terms of electromagnetic wave absorption. This material's minimum RL at 9.75 GHz is -41.38 dB, while its effective absorption bandwidth (from 8.40 to 11.48 GHz) is 3.08 GHz (from 8.40 to 11.48 GHz) makes it an ideal contender for high-efficiency electromagnetic wave absorbers. The combination of conductive polymer, porous magnetic nanoparticles, and rGO improves impedance matching and boosts the material's attenuation constant.[43]

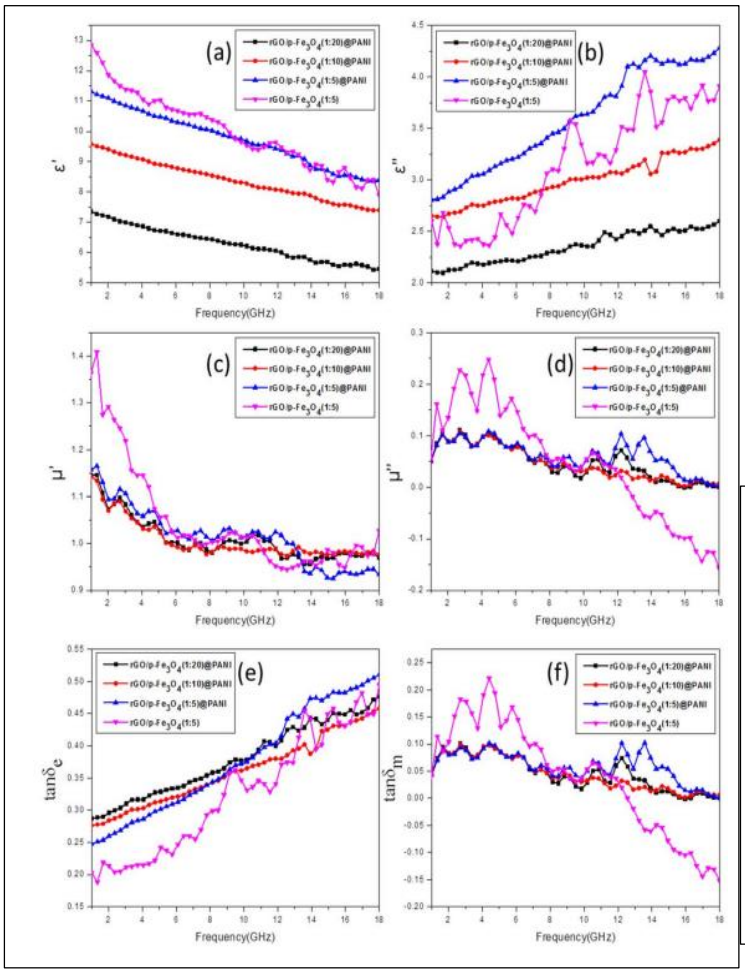

Figure 54. (a) The real and (b) imaginary parts of the permittivity of the samples; (c) the real and (d) imaginary parts of the permeability of the samples; (e) dielectric and (f) magnetic loss tangent of the samples

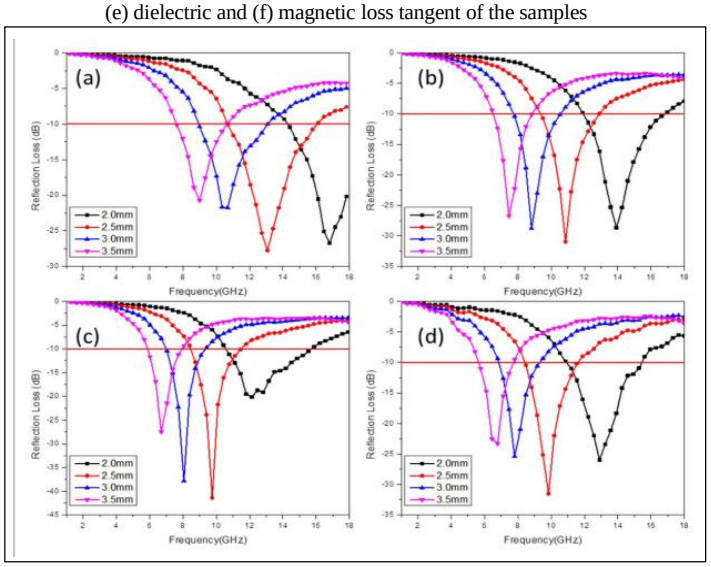

Figure 55. Reflection loss curves of(a) rGO/p-Fe3O4(1:20)@PANI, (b) rGO/p-Fe3O4(1:10)@PANI, (c) rGO/p-Fe3O4(1:5)@PANI, (d) rGO/p-Fe3O4(1:5) samples with different thicknesses

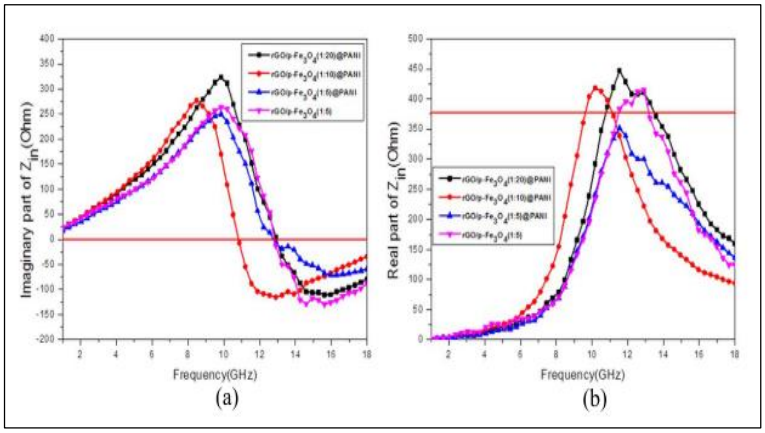

Figure 56. (a) Imaginary impedance and (b) real impedance of complex impedance Z_{in} of the samples.

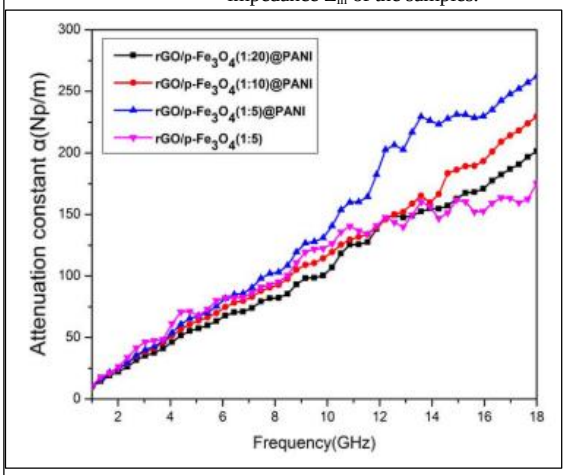

Figure 57. Attenuation constant of α of the samples

Sandwich-like rGO/CuS/Polypyrrole Nanoarchitectures and other polymer composites

Previous research has established that reduced graphene oxide (rGO) advances in the field of Electromagnetic Absorption (EA). However, the high permittivity of rGO always outperforms the impedance, resulting in increased electromagnetic wave reflection on the surface. Here discuss the easy two-step synthesis of sandwich-like rGO/CuS/polypyrrole (PPy) nanoarchitectures. The experimental results indicate that a paraffin composite comprising 10% rGO/CuS/PPy can significantly improve EA performance in terms of bandwidth and intensity. A minimal reflection loss (RL) of 49.11 dB is possible. Additionally, the effective bandwidth is 4.88 GHz. The finding indicates that the rGO/CuS/PPy nano architectures as constructed will be a potential EA material.[44]

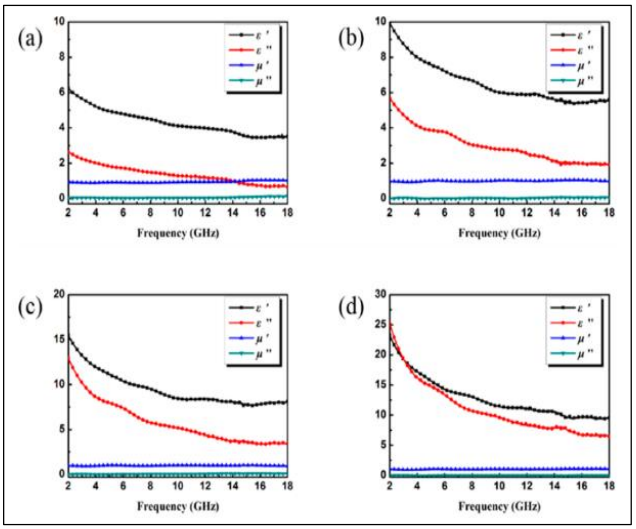

Figure 58. Complex permittivity and permeability of rGO/CuS/PPy with the filler loading of 5 wt.% (a), 10 wt.% (b), 15 wt.% (c), and 20 wt.% (d)

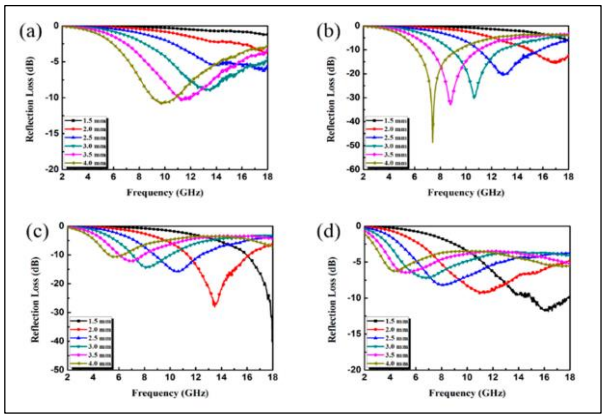

Figure 59. RL curves of paraffin composites containing 5 wt.% (a), 10 wt.% (b), 15 wt.% (c), and 20 wt.% (d) of rGO/CuS/PPy.

SEM, TEM, and other studies revealed that dense PPy particles have evenly polymerized on the surface of rGO/CuS in the ternary composites, producing a "sandwich" structure. At a matched thickness of 4.0 mm, the rGO/CuS/PPy mixture has exhibited a maximum RL of 49.11 dB. The matched thickness of 2.5 mm has resulted in a 4.88 GHz effective EA band. While increasing the filler loading to 15%, the highest RL value shows 39.55 dB, and the matching thickness shows 1.5 mm. The effective EA band was 4.84 GHz when the matching thickness was 2.0 mm. Multiple components and the unique structure of rGO/CuS/PPy increase not only the dielectric loss capacity and impedance matching properties but also the interface polarization effect, resulting in improved EA performance. [44],[45],[46]

EM wave absorber polymers with low density (e.g., polyaniline (PANI), polypyrrole (PPY), and even foam-like polyacetylene (PAE) can solve EMA materials' issues. Its applicability at high frequency is limited because the single polymer EM wave absorber cannot produce considerable electric/magnetic loss. With its bigger surface area, more atoms, multi-reflection, and thus larger dielectric or magnetic loss, nanostructure materials may be one of the most promising materials for compensating for the above shortcomings and improving EM wave absorption capabilities. Making great EM wave absorption materials from polymers and nanomaterials may be an ideal method.

A thin EM wave absorber is made of nanomaterials with low density and strong electric/magnetic loss. Highly efficient polymer-based nanocomposites with low density, thin thickness, broad absorption band, and high EM wave loss are being developed. Polymers such as epoxy resin, polyurethane, and rubber serve as matrices for polymer-based nanocomposites while also improving EM wave absorption.[5] Nanocomposite matrix based on epoxy resin To increase EM wave reflection loss, a polymer can be used as a matrix. It is commonly employed in polymer-based nanocomposites because of its good mechanical, chemical, and thermal stability. [47]

Table 20. EM wave absorption properties of epoxy resin-based nanocomposites

	Absorber	D (nm)	d (mm)	$e^{(a)}$	$\ell^{(a)}$	$tg\delta_e$	$tg\delta_\iota$	Df	$R_{L,max}$ (f_{im})
1	8 vol.% $BaTiO_3$	40–60	4	7.5	0	0.5	0	8 (10–18)	19 (12.9)
2	80 wt% α-Fe/Y_2O_3	30	4	0.6	1.1	0.05	0.55	1.2 (2–3.2)	36 (2.6)
3	80 wt% α-Fe/Fe_3B/Y_2O_3	20	4	0.6	0.55	0.04	0.44	2.1 (3.5–5.6)	33 (4.5)
4	51 vol.% Fe_3N/Y_2O_3	Fe_3N 10 Y_2O_3 30	7.05	2	0.5	0.12	0.28	0.6 (1.5–2.1)	55 (1.8)
5	80 wt% $Fe_{0.33}Co_{0.67}$/Y_2O_3	$Fe_{0.33}Co_{0.67}$ 20 Y_2O_3 10	4.3	0.5	0.8	0.036	0.47	1.4 (2.5–3.9)	55 (3.2)
6	75 wt%α-Fe/C(a)	100–1000	2.5	0.4	1	0.033	0.59	3 (4–7)	58 (5.9)
7	75 wt% Fe_2B/C(a)	100	1.6	0.7	0.6	0.057	0.43	4 (8.4–12.4)	60 (10.7)
8	75 wt% Y_2Fe_{17}/C(a)	20	1.3	0.6	0.5	0.06	0.5	5 (13–18)	48 (17)
9	16.7 wt% Fe/MWNT	40	1.2	41	1.9	1.37	0.97	16 (2–18)	25 (11)
10	44.4 wt% Ni/Ag	7.9	1.8	9	0	0.73	0	2.4 (9.7–12.1)	24 (10.9)
				0	4	0	0.67	5.3 (28.9–34.2)	27 (31.3)
11	M[b]: 10 wt α-MnO_2	50–60	2	6	0	0.4	0	9 (9–18)	29 (15.8)
	A[b]: 30 wt% CB	20–30	3						
12	M[b]: 0.4 wt% MWNT	10–25	1.9	0.6	0	0.11	0	4 (8.2–12.4)	47 (9.8)
	A[b]: 1.6 wt% MWNT		1.4	5.5	0	0.88			

Table 21. EM wave absorption properties of other polymer-based nanocomposites

	Absorber	*D* (nm)	*Matrix*	*d* (mm)	ε'^{MAX}	μ'^{MAX}	$tg\delta_e$	$tg\delta_\mu$	Df	$R_{L,max}$ (f_m)
1	5wt%SWNT	1.2-1.8	PU	2	3.75	0	0.3	0	2.6 (7.5–10.1)	21.9(8.8)
2	65%Fe/Fe_2O_3	20	PU	1.7	0	2.4	0	0.11	3(8–11)	27.5(10)
3	7wt% *ZnO*	20	PET	1	0.13	0	0.07	0	2 (10–12)	12.28(10.9)
4	5.% Fe_3 Ni-MWNT	260	PPESK	0.9					4 (9.5–13.5)	27.5(10.9)
	ZnCoBa Iron particles	65	CSPER	0.5					5.6(8.4-14)	28.5(10.9)
5	M:18wt%NTP and 62wt%MMP A:85wt%MMP		HNBR	0.65 0.55					7.1 (2.5–3.9)	12 (11.2)
6	4wt%MWNT/PANI-pTsA 10wt%*α*-Fe2O3	20-50 70	PMMA PANI		100 2.4	9 0.66	9 0.4	0.06		(8.2) 25(16)
7	75 wt% BF	50-70	PANI		29		2.9		5.6 (12.4–18)	27.5 (18)
8	A:CNT,etc, M:PPY fabric		PU	11.6					15 (3–18)	25.5(6.3)

Conducting polymers as nanocomposites' absorbent components

EM wave absorption characteristics with a broad absorbing breadth and changeable absorbing frequency have been discovered in conducting polymers. Nanomaterials, on the other hand, exhibit substantial electric or magnetic losses. One of the best ways to build optimal EMwave absorbers is by combining conducting polymers and nanomaterials (Table 2). using PANI-pTsA coated MWNTs with PMMA to create thermoplastic nanocomposites. Composites with PANI-pTsA-coated MWNTs performed better in the polymer matrix than those without. The research studied the EM wave absorption capabilities of c-Fe_2O_3/protonated PANI nanocomposites with varied c-Fe_2O_3 loadings. A large absorption band with reflection loss of 10 dB between 13 and 17 GHz has been identified in nano-composite materials containing 10% c-Fe_2O_3.study has investigated the EM wave absorption characteristics of BF/PANI composites synthesized by emulsion polymerization at 12.4–15 GHz (see figure). The 75 wt% BF composites had high absorption efficiency above 20 dB in the test frequency range and 27.5 dB at 18 GHz. In PANI, strong polarization caused the dielectric loss, whereas, in BF, magneto crystalline anisotropy caused the dielectric loss, and interface polarization caused multi scattering leading to high absorption efficiency. With the impedance matching layer made of PPY textiles with various surface resistances, here present constructed multi-layer EM wave absorbers. Using a six-layer composite with a surface resistance of 15.9 S cm^2 and a PPY layer with a surface resistance of 5.2 to 8 GHz, the reflection loss was over 15 dB from 5.2 to 8 GHz and above 20 dB from 8 to 18 GHz for the 11.6 mm thick sample.[5]

Innovative approaches to design the ideal absorber, such as the simultaneous action of both dielectric and magnetic materials with disordered structure, core-shell, and multi-layer structure, will be discussed. EM wave absorption is a challenging field that requires innovative approaches to design the ideal absorber. RL above 10 dB (10 percent incident wave is reflected) is wider than RL above 20 dB (1 percent incident wave is reflected). For example, 16.7% Fe/MWNT shows RL above 10 dB between 2 and 18 GHz, but only between 4.5 and 5.5 GHz and 10 and 15 GHz, and only between 10 and 15 GHz, RL above 20 dB was observed. A simplex absorption frequency band limits the usage of current materials in both low (MHz) and high frequency (GHz) applications (GHz or more). Polymer-based nanocomposites with core/shell or multilayer architectures might alleviate these issues. It is also possible that future materials will be multi-functional and intelligent EM absorbers. Intelligent components in nanocomposites, for example, can automatically change the matching frequency to the surroundings.[5]

Carbonyl iron and polychloroprene composites film

The carbonyl iron particles have been distributed in a polychloroprene rubber (CR) matrix as a microwave absorption composite film. Films created with an external magnetic field have superior microwave absorption characteristics compared to films made with a general magnetic field. An external magnetic field thin film with a thickness of just 0.54 mm displays the least reflection loss of -15.98 dB and less than -10 dB for the frequency range of 11.4 to 14.8 GHz. To make a thinner and lighter microwave absorber, the composite thin film that can be

formed under an external magnetic field has been found to have good microwave absorption capabilities.[48]

Microwave absorber composites distributed in a polymer matrix have recently reported high absorbing characteristics but only 1mm in total thickness.

An alternating dielectric polymer film and conducting layer multilayer structure with a 4mm thickness has been reported to successfully absorb electromagnetic wave radiation over a wide range of wavelengths. [49]

Nanocomposite materials are made of thermoplastic polyurethane and 20wt.% exfoliated graphite has been created by researchers. In general, the composites had a shielding efficiency of -20 dB, making them appropriate for industrial use. The modeling findings revealed that a 1 mm thick layer may produce significant narrowband electromagnetic wave attenuation (>-15 dB). Anisotropy and particle dispersion homogeneity in the matrix have been presented in this work.[48]

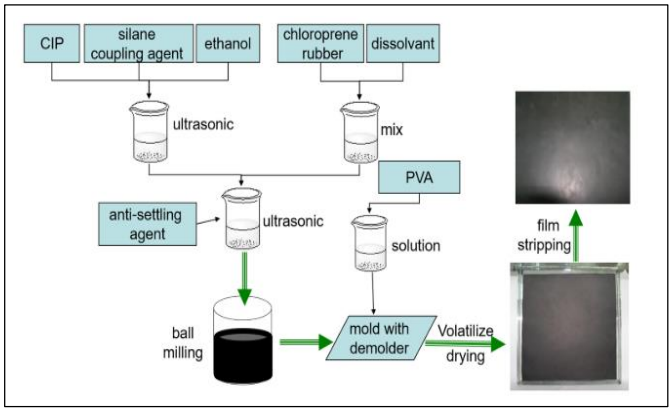

Figure 60. The preparation process of the composite film

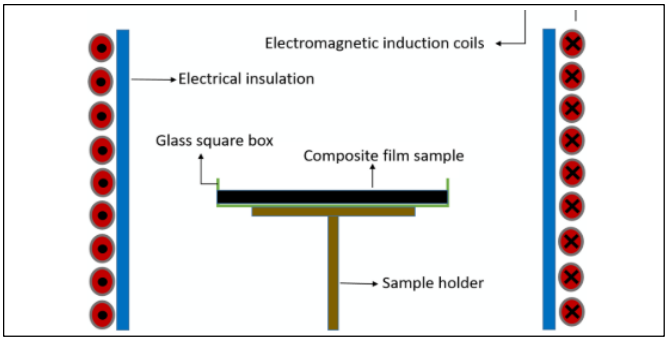

Figure 61. Schematic diagram of the composite film dried apparatus with a static magnetic field produced by electromagnetic induction coils

Figure 61 depicts the magnetic direction perpendicular to the film produced by the same procedure. Without magnetic field films (Fb) /and with magnetic field films (Fc)

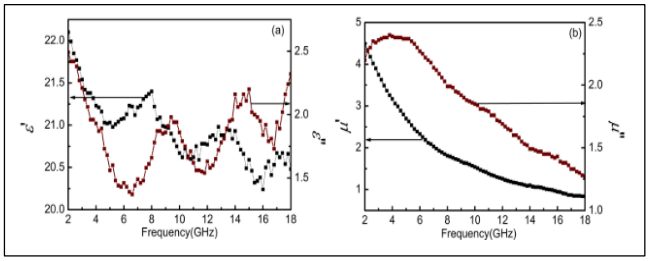

Figure 62. The relative complex permittivity and permeability of carbonyl iron-paraffin wax composites vs frequency.

Ferromagnetic particles distributed in an insulating polymer matrix can reduce the eddy current effect.

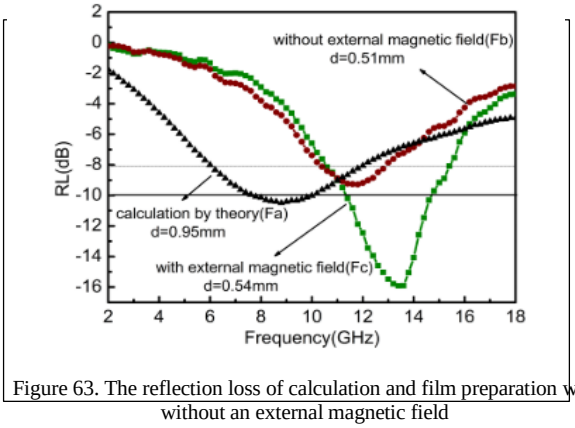

Figure 63. The reflection loss of calculation and film preparation with and without an external magnetic field

Above presents the reflection loss of the CIP-CR composites films with 38.5 mass % CIP made with, and without external magnetic field, and the calculation of the 85mass% CIP and paraffin composites, which have been defined as Fb, Fc, and Fa, respectively. The calculation reflection loss (RL) curve is obtained from the relative complex permittivity and permeability, utilizing transmission line theory[48]

Dispersed in CR with external magnetic field technique, CIP exhibits good microwave absorption qualities with the lowest RL of -15.98 dB and bandwidth of RL value less than -10 dB of 3.4GHz, and with a thickness of just 0.54 mm, RL exceeding -8.0 dB. It has better absorption characteristics than films formed without an external magnetic field due to increased anisotropy and reorganization of the magnetic domain caused by the external magnetic field. As thinner electromagnetic wave absorbers, our CIP/CR film manufactured in an external magnetic field can be used.[48]

Natural-fiber reinforced composites (by incorporating powdered activated carbon) [50]

Vacuum-assisted resin transfer molding (VARTM) has been used to create kenaf fiber–polyester composites containing activated carbon powder. The product shields electromagnetic interference (EMI). This process removes the lignin and extractives from the kenaf fibers. The PAC has retted fibers in water. It can be calculated using the Brunauer-Emmett-Teller (BET) specific surface area analysis. A larger PAC loading resulted in a higher BET. The transmission energy of the composites has been measured by irradiating them with electromagnetic waves ranging from 8 GHz to 12 GHz [50]. The EMI shielding efficacy has been reported from 41.4 percent to

76.0 percent, 87.9 percent, and 90.0 percent when the PAC content grows from 0% to 10.0%, 20.5%, and 28.9%. Also, EMI absorption has been reported from 21.2 to 31.7, 44.7, and 64.0 percent. The composite's EMI absorption/shielding ratio at 28.9% PAC loading increased by 37.1 percent compared to the control sample. The use of PAC in composites was shown to effectively absorb electromagnetic waves, reducing secondary electromagnetic pollution.

Table 22. Contents of the composites (PAC = powdered activated carbon)

COMPOSITE / DENSITY	THICKNESS	CONTENT(%)		
		FIBER	PAC	RESIN
Fiber/polyester 1159.4(44.5)	2.6	66.7	0.0	33.3
Fiber/PAC10/polyester 1157.3 (15.1)	3.5 (0.1)	64.2	10.0	25.8
Fiber/PAC20/polyester 1064.7 (20.4)	4.2 (0.1)	57.9	20.5	21.7
Fiber/PAC30/polyester 1036.2 (18.8)	4.8 (0.2)	47.1	28.9	24.1

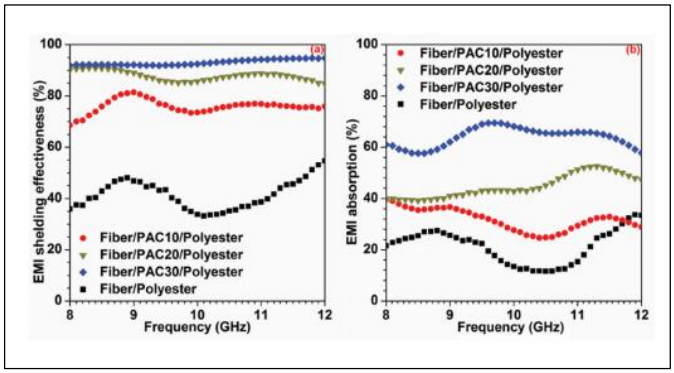

Figure 64. EMI shielding effectiveness (a) and absorption (b) of the four composites.

Table 23. EMI shielding and absorption of the four composites.

Composite	EMI Shielding (%)	EMI Absorption (%)	EMI Absorption/Shielding (%)
Fiber/PAC10/polyester	76.0 (2.6)	31.7 (4.2)	41.8 (5.7)
Fiber/PAC20/polyester	87.9 (1.8)	44.7 (4.4)	50.9 (5.4)
Fiber/PAC30/polyester	93.0 (1.1)	64.0 (3.7)	68.7 (4.1)
Fiber/polyester	41.4 (5.5)	21.2 (6.5)	50.1 (10.3)
Increment (%) c	124.6	201.7	37.1

Composites made of kenaf, PAC, and polyester utilizing VARTM technology. The BET-specific surface area study demonstrated an improvement in PAC loading efficacy. The EMI shielding tests ranged from 8 GHz to 12 GHz. The EMI shielding and absorption has been reported from 41.4 to 93.0 percent, and 21.2 to 64.0 percent, respectively, as the PAC content grow from 0 to 28.9%. The results have revealed that PAC was more successful at absorbing EMI signals than reflecting them, reducing secondary electromagnetic pollution. However, adding PAC have reduced the mechanical and dynamic mechanical characteristics. More work must be planned to improve the composites' characteristics.[51]

Nanostructured Barium Titanate/Carbon Nanotubes Incorporated Polyaniline

Structures produced by barium titanate/carbon nanotubes integrated polyaniline are good for strengthening electromagnetic absorption. To create the CNTs/$BaTiO_3$/PANI or CBP ternary composites, a simple and versatile approach combining sol-gel, in situ polymerization, and mechanical processing has been presented here. A vector network analyzer has been used to study the dielectric and microwave absorption characteristics of CNT/$BaTiO_3$/PANI (CBP) composites. The CNTs/$BaTiO_3$/PANI composites with 3D conductive network topologies have exceptional electromagnetic absorption capabilities, perhaps due to their excellent impedance matching behavior, reduced dielectric loss, and new synergistic impact. Also, the "geometrical effect" of the composite may have aided in absorbing the incoming electromagnetic radiation. In this composite, the mass ratio of CNTs/$BaTiO_3$ to PANI is 2:3, and the absorption bandwidth with a reflection loss of 10 dB ranges from 7.5 to 10.2GHz.

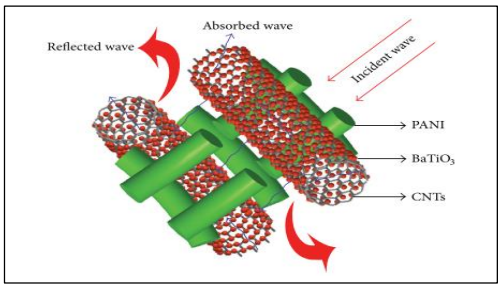

Figure 65. Electromagnetic wave absorbing mechanism of CBP composite

Table 24. Composite absorbing material of CBP with a different mass ratio

SAMPLES	COMPOSITION
CBP_3	CNTs/$BaTiO_3$: PANI (mass ratio) = 4 :1
CBP_3	CNTs/$BaTiO_3$: PANI (mass ratio) = 3:2
CBP_3	CNTs/$BaTiO_3$: PANI (mass ratio) = 2 :3
CBP_3	CNTs/$BaTiO_3$: PANI (mass ratio) = 1:4

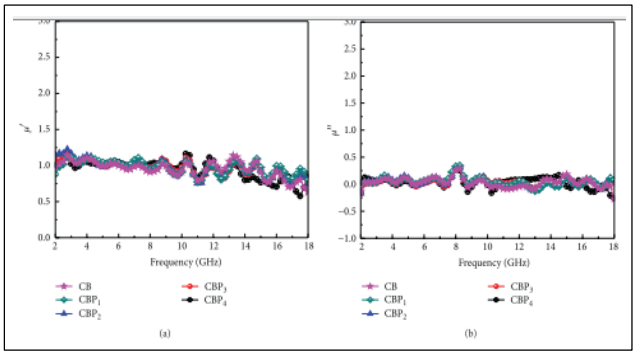

Figure 66. Complex permeability of samples: (a) real part and (b) imaginary part

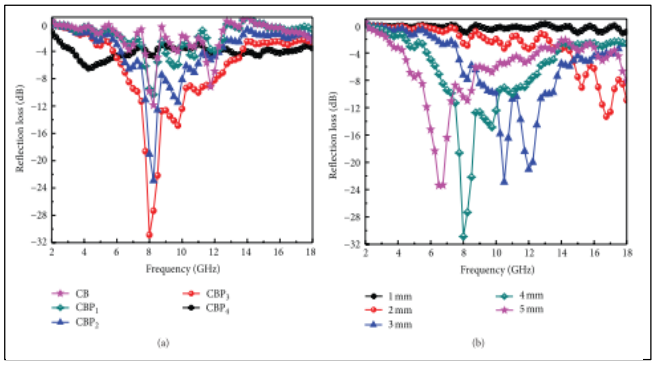

Figure 67. (a) Reflection loss of samples with the thickness of 4mm and (b) reflection loss of CBP3 with different thicknesses.

Easy and flexible barium titanate/carbon nanotubes including polyaniline composites with 3D conductive network structures have been successfully made. The presence of CB and PANI, as well as the synergistic and geometrical effects of the microstructure, all contribute to the remarkable performance of CBP composites. The CBP3 (CB: PANI = 2:3) has the finest microwave absorption capabilities. At 8GHz, CBP3 has a maximum reflection loss of -30.9 dB with a 4mm thick sample layer and a 30wt% paraffin wax filler loading, and the bandwidth with a reflection loss less than -10dB covers 7.5 to 10.2GHz. So it's logical to suppose they can make futuristic microwave absorbers.[52]

Poly(3,4-ethylenedioxythiophene) Nanofiber-Decorated Graphene Sheets

Graphene sheets (GNs) have strong conductivity but poor EM wave absorption. poly (3,4-ethylene dioxythiophene) PEDOT nanofibers were deposited on the surface of GNs, where the remaining defects and groups function as active sites for the deposition of PEDOT nanofibers. The SEM photos show PEDOT nanofibers effectively polymerized on GN surfaces. The PEDOT nanofibers is 15 to 50 nm in diameter and hundreds of nanometers long. Graphene, PEDOT, and GNs-PEDOT also presented for EM wave absorption. GNs-EM PEDOT's wave absorption characteristics are enhanced compared to pure graphene and PEDOT. The greatest RL is -48.1 dB at 10.5 GHz with a 2 mm thickness. RL values below -10 dB had an absorption bandwidth of 9.4 GHz (5.8–12.3, 12.9–15.8 GHz) in 1.5–3 mm thickness[53]. The improvement is due to PEDOT alteration and nanofiber structure. On one side, putting PEDOT nanofibers on graphene reduces its conductivity and improves impedance matching. However, due to their unique structure, PEDOT nanofibers have high specific surface areas, giving more active sites for EM wave reflection and scattering. Thus, the non-covalent deposition of conducting polymers on GNs provides an effective technique for creating robust EM wave absorbers.[54]

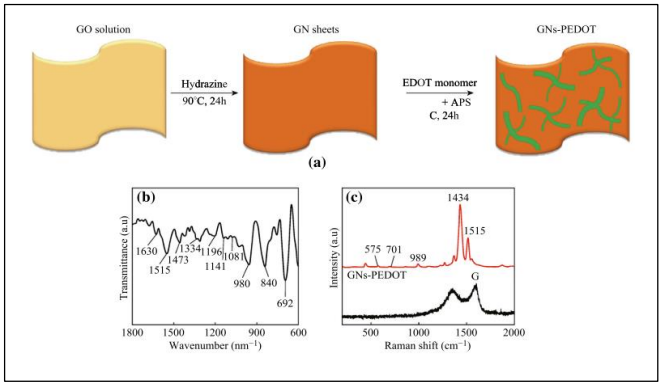

Figure 68. a schematic illustration of GNs-PEDOT. b FTIR spectra of GNs-PEDOT. c Raman spectra of GO and GNs-PEDOT

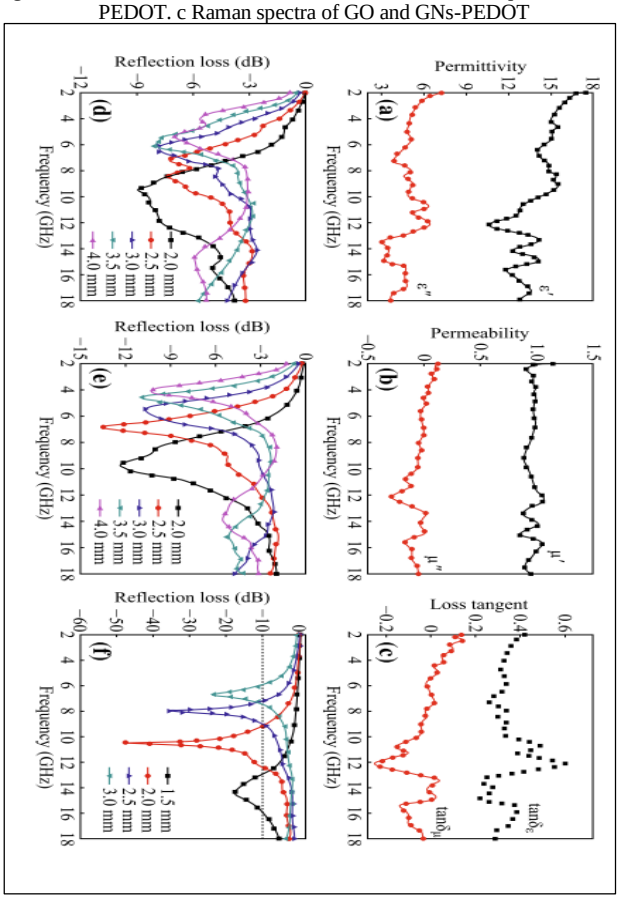

Figure 69. The complex relative permittivity (a), permeability (b), and loss tangent (c) of GNs-PEDOT. Reflection loss curves of d GNs, e PEDOT, and f GNs-PEDOT

Strong and thermostable polymeric graphene/silica textile

Here presents a unique technique to create robust and thermostable polymeric graphene/silica textile composites for practical microwave absorption applications. A novel silica

cloth paired with a freeze-drying process is used to achieve a homogenous configuration, allowing Reduced Graphene Oxide (RGO) to build three-dimensional conductive frameworks in situ. Because silica textiles and thermoset polymers coexist, these integrated bi-matrices provide significant mechanical and thermal reinforcement to composites. The as-fabricated lightweight composites (1 g/cm^3) had 40 MPa tensile strength and 95 percent mass retention in air, with a microwave absorption peak at -36 dB and efficient absorption in the complete X-band at low filler loading (4.1 wt. percent RGO). The results imply that the outstanding overall performance permits such innovative polymeric composites to be used for practical microwave absorption.[55]

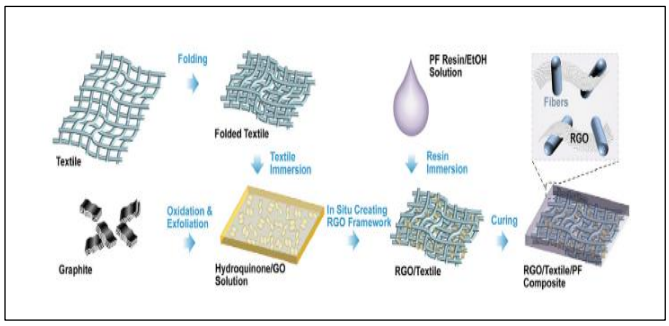

Figure 70. Scheme of the procedures for RGO/silica textile/PF composites

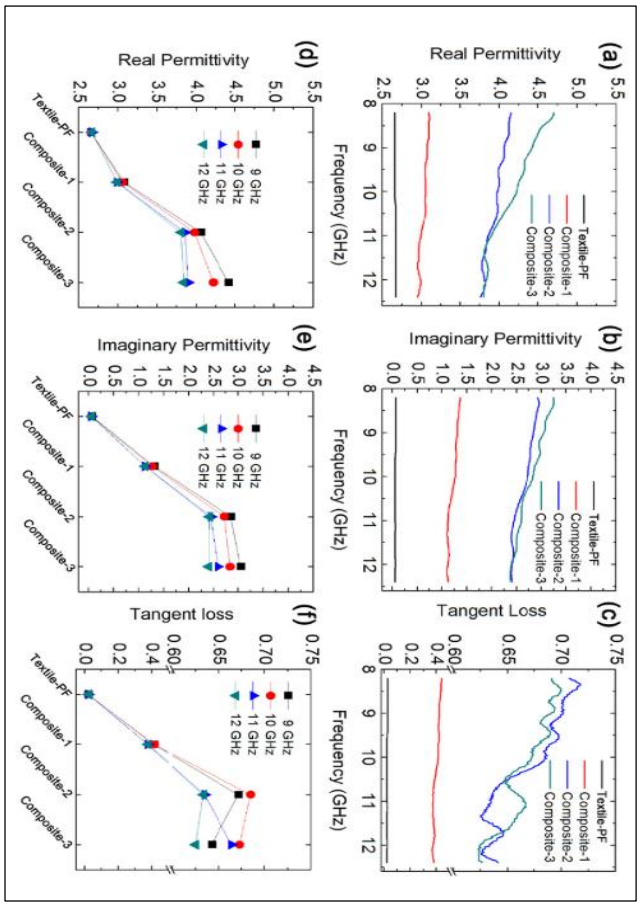

Figure 71. Real (a), imaginary permittivity (b), and tangent loss (c) of the samples marked; Real (e), imaginary permittivity (e), and tangent loss (f) at various frequencies

A flexible thermostable composite might be created by replacing PF resins with high thermostable polymers (for example: Polyimide).

Here shows the RGO/silica textile/PF composites for effective microwave absorption applications. The silica cloth contributed significantly to the composites' tensile strength of 40 MPa and heat stability beyond 225 celcius (95 percent mass retention in the air). At -36 dB, efficient microwave absorption has been detected over the full X-band. The results show that the RGO/silica textile/PF composites have appropriate overall performance for practical microwave absorption applications. The new work also proposes a simple and universal technique for scale production of graphene-based composites, which might be applied in many domains.[55]

Three-dimensional (3D) α-Fe_2O_3/polypyrrole (PPy) nanocomposite

A simple one-pot polyreaction produced lightweight 3-dimensional reticulated α-Fe_2O_3/PPy hybrids. Complexity and microwave attenuation measurements imply that the mass ratio of α-Fe_2O_3 added controls the dielectric characteristics of PPy. The interface capacitor-like structure accounts for the two complicated permittivity resonance peaks. The nonlinear resonance behavior of α-Fe_2O_3/PPy wax composites have been explained using an analogous circuit model[56]. The inclusion of α-Fe_2O_3 have adjusted the dielectric constant to maximize microwave absorption. The effective bandwidth (RL) of α-Fe_2O_3/PPy wax composites has been increased by -10dB up to 5.0GHz. The numerical technique has suggested to compute the appropriate thickness for minimum RL at the predicted frequency. Another advantage is that it is possible to acquire the appropriate thickness directly.

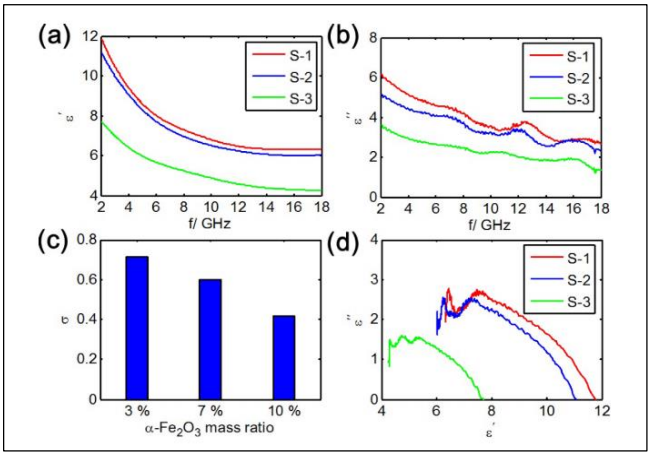

Figure 72. The frequency dependence of dielectric properties for the paraffin-based composites (10 wt%): (a) real permittivity; (b) imaginary permittivity; (c) conductivity fitted by Debye theory and (d) cole-cole plots.

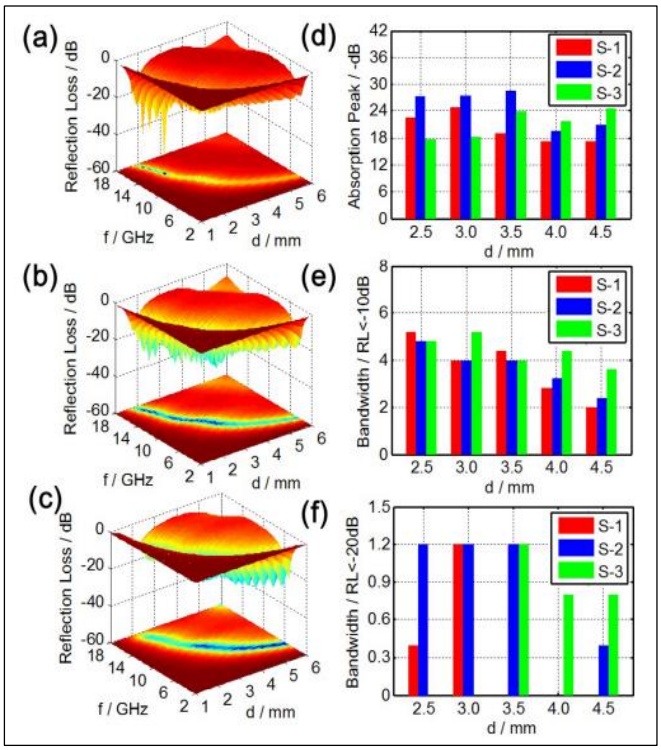

Figure 73. Three-dimensional plots of RL values for paraffin-based composites: (a) S-1, (b) S-2, and (c) S-3; EA performance comparison of three samples: (d) absorption peaks, (e) RL ≤ −10 dB peak width and (f) RL ≤ −20 dB peak width

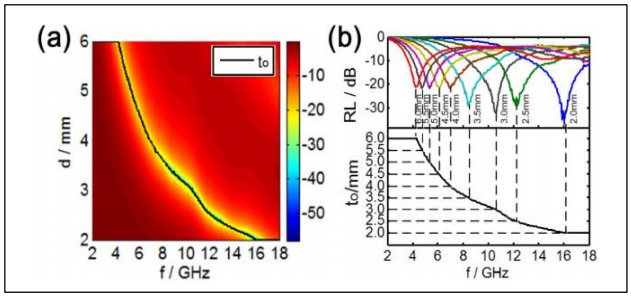

Figure 74. Numerically calculated optimum thickness (a) of S-2 for minimum RL at expected frequency; optimum thickness and EA performance at corresponding thickness (b).

Optimal thickness (2-6 mm) for minimal RL using the numerical technique at a fixed frequency when the frequency is below 4.8 GHz, the ideal absorber thickness is 6 mm. With a frequency of 16.4 GHz, the to falls to 2 mm. After 16.4GHz, the top is 2 mm.[57]

Coating (p(HEMA-co-BA)-Fe3O4) with Self-Healing Properties

A self-healing electromagnetic absorption coating (p(HEMA-co-BA)-Fe_3O_4) has been synthesized by copolymerizing HEMA, BA, and functional monomers (Fc/CD-Fe_3O_4 complexes). Excellent adherence to the substrate, moderate hardness, and good absorption over a broad range of radar bands.

More significantly, a modest amount of water may effectively cure fractures in the p(HEMA-co-BA)-Fe_3O_4 covering. During the self-healing process, the coating's electromagnetic absorption capacity has restored. The self-healing theme was the Fe_3O_4 particle-polymer matrix interaction. This p(HEMA-co-BA)-Fe_3O_4 coating has considerable promise in military , medical and civic applications.[58]

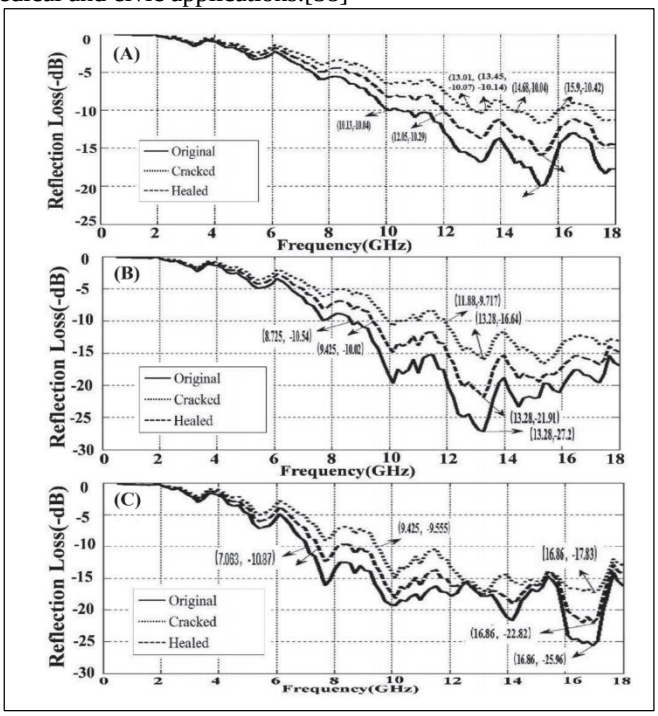

Figure 75. Self-healing of microwave absorptive properties of p(HEMA-co-BA)-Fe3O4 coating. A) 3 mm; B) 4 mm; C) 5 mm.

The frequency increases the relative magnetic permeability (tan δμ). Tan δε and tan δμ are proportional to the material's loss capacity. A high tangent value indicates a high absorption capacity. These RL values are derived from tan δε and tan δμ at a certain thickness.[58]

Table 25. Absorption bandwidth (RL < −10 dB) with different thicknesses.

		3mm	4mm	5mm
Absorption bandwidth (RL < −10 dB)	Original	6.87	9.725	10.937
	Cracked	2.17	6.45	8.575
	Healed	5.95	8.55	10.388
Loss rate		68.41%	33.67%	21.59%
Self-healing efficiency		86.6%	87.91%	94.98%

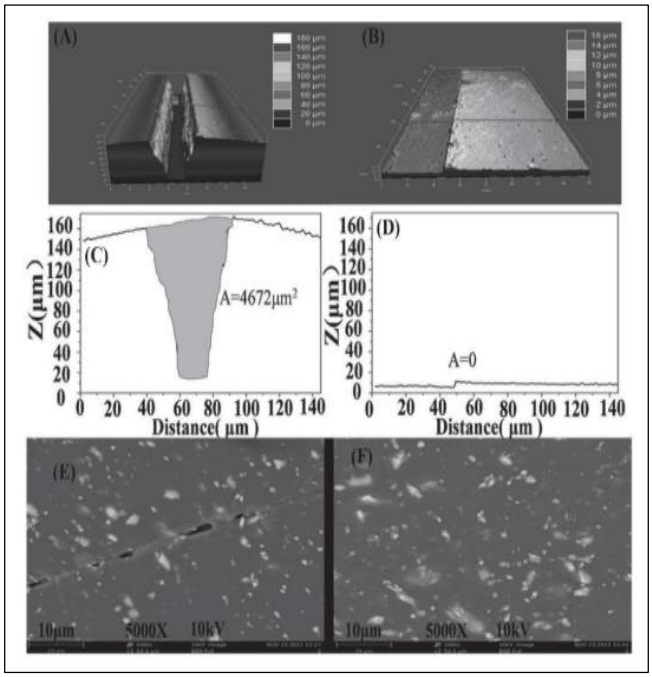

Figure 76. A–D) Self-healing behavior of p(HEMA-co-BA)-Fe3O4 coating. LSCM photos of coating with one crack on the surface (A, C) before and (B, D) after healing. E–F) SEM photos of coating with one crack on the surface (E) before and (F) after healing.

Conjugated polymer-based composites

In terms of MAM (Microwave Absorbent Materials), conjugated polymer (CP)-based composites look to be promising low density and high performance[9]. These breakthroughs include the rational design of the microstructure of pure conjugated polymers and tunable chemical integration with magnetic ferrites, magnetic metals, transition metal oxides, and carbon materials are summarized in this study. It is important to control EM characteristics, increase characteristic impedance matching, and establish diverse loss mechanisms in CP-based MAMs. To meet the high demands of the next generation of MAMs, the examples in this study will give fresh insights into composite design and processing.[59]

Recent advances in conjugated polymer-based composites as microwave absorbers are reviewed. Because some CPs with unique microstructures like PANI micro rods, PANI nanoparticles, multi-shelled PEDOT hollow microspheres, and highly uniform core-shell PPy@PANI - displayed significantly enhanced microwave absorption when compared to their conventional counterparts, some studies concluded that rational design on the microstructure of conjugated polymers (CPs) could regulate their EM properties and improve the matching of characteristic impedance. More and more research has been done on heterogeneous carbon-based composites with different magnetite and magnetic elements for microwave absorption. Complementary and synergetic effects, as well as other loss mechanisms (e.g., multiple polarization relaxations), might result from combining CPs with inorganic additions. Components with secondary magnetic or dielectric characteristics can be added to CP-based composites to improve the attenuation of incident EM waves. The use of ternary and quaternary CP-based composites for high-performance MAMs is gaining popularity. They were also used in multi-layer MAMs for practical microwave absorption. The sensible organization of multi-layer MAMs contributed greatly to response bandwidth expansion. [59]

However, there is still a gap between research and industry applications of CP-based composites. Because present composites cannot meet the specific requirements for MAMs, additional work in this sector is necessary. As a result, most researchers use cumulative absorber thicknesses or multi-layer configurations to widen the response frequency range. A reasonable microstructure design can enhance microwave absorption in pure CPs, but not in CP-based composites. To achieve optimal microwave absorption performance, it will be necessary to create multi-compound composites with certain microstructures (e.g., hollow, yolk-shell, reduced particle size). The second issue is that much research is focused on improving microwave absorption independent of other factors. Low density and low loading are critical in practical applications, notably in aeronautics and astronautics. Using ultra-light additives for diverse CP-based composites makes sense based on functional comparability alone. As a result, the durability of CP-based composites should be considered. In conclusion, CP-based composites show promise as MAMs, even though the study is very young. A promising future is predicted for innovative CP-based composites with perfect compositions and microstructures.[59]

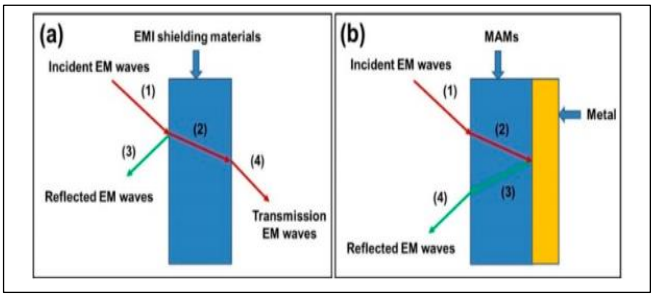

Figure 77. The evaluation models of (a) conventional electromagnetic interference (EMI) shielding and (b) microwave absorption. MAM: microwave-absorbing material.

Pure CPs, magnetic ferrites/CP composites, magnetic metal/CP composites, transition metal oxides/CP composites, carbon/CP composites, multi-compound CP-based composites, and multi-layer CP-based composites can be further studied in this work.[59]

Table 26. Performance comparison of representative CP-based MAMs.

Entry	Absorbers	Thickness	MaxRLand frequency	Bandwidth over -10dB(range,GHz
1	3D PPy aerogel	3.0	−22.5 dB at 12.0 GHz	5.0 (10.0–15.0)
2	PANI nanoparticle	2.0	−18.8 dB at 17.2 GHz	3.9 (14.1–18.0)
3	Fe_3O_4 nanoparticle/PPy	1.7	−35.1 dB at 16.7 GHz	2.1 (15.9–18.0)
4	Fe_3O_4 microspheres/PANI	3.0	−31.3 dB at 9 GHz	2.2 (7.6–9.8)
5	$BaFe_{12}O_{19}$/PANI	2.0	−20.0 dB at 14.5 GHz	4.0 (12.8–16.8)
6	Ni/PANI	1.0	−23.0 dB at 17.8 GHz	2.5 (15.5–18.0)
7	α-MoO_3/PANI	2.0	−34.0 dB at 16.8 GHz	2.8 (15.2–18.0)
8	MCNT-COOH/PPy	3.5	−16.0 dB at 11.5 GHz	4.5 (9.5–14.0)
9	Graphene/PANI	2.5	−45.1 dB at 12.9 GHz	5.4 (10.6–16.0)
10	$0.9BaFe_{12}O_{19}/0.1Y_3Fe_5O_{12}$/PANI	2.9	−40.8 dB at 9.9 GHz	5.5 (6.8–12.3)
11	Graphene/$CuFe_{10}Al_2O_{19}$/PANI	2.5	−63.6 dB at 11.5 GHz	4.5 (8.0–12.5)
12	$NiFe_2O_4$/graphene/PEDOT	2.5	−50.5 dB at 12.5 GHz	5.3 (11.0–16.3)
13	Graphene/Fe_3O_4/SiO_2/PANI	2.5	−40.7 dB at 12.5 GHz	5.8 (10.5–16.3)
14	Fe_3O_4-PANI layer/PANI layer	1.0	−42.0 dB at 29.27 GHz	11.8 (25.5–37.3)

Fe_3O_4@polyaniline yolk-shell micro/nanospheres as bifunctional materials

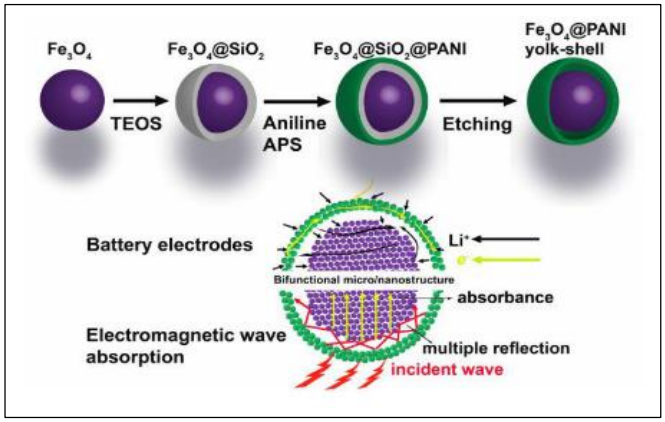

Figure 78. Fe_3O_4@polyaniline yolk-shell micro/nanospheres synthesized by a facile silica-assisted solution phase method

Fe_3O_4/polyaniline composite with yolk-shell micro/nanostructure (FPys) has been effectively produced by silica-assisted in situ polymerization and etching. X-ray diffraction (XRD) and X-ray photoelectron spectroscopy (XPS) have been used to study the FPys composites' structure and chemistry. SEM and TEM images corroborate the goods' yolk-shell shape. FPys electrodes outperform bare Fe_3O_4 micro/nanospheres and Fe_3O_4/PANI anodes in terms of capacity, cycle stability, and rate capability. [60]

The FPys micro/nanostructures have been made of Fe_3O_4/PANI composites with a yolk-shell arrangement. The produced sample performed well as both LIB anodes and electromagnetic wave absorbers. The FPys cell has a reversible capacity of 982 mAhh g^{-1} after 50 cycles at 100 mA g^{-1}. At 1000 mA g^{-1}, the capacity is 734.6 mAhh g^{-1}. The FPys sample exhibits increased dielectric and magnetic loss between 2.0-18 GHz. Reflection losses as low as -10 dB may be attained with absorber thicknesses as little as 1.9 to 5.0 mm in the 6.3-18.0 GHz range. The hierarchical micro/nanostructures give the bifunctional characteristics. This method may be used to synthesize various multifunctional materials. [60],[61]

NiS_2@rGO nanosheet wrapped with PPy aerogel as sandwich-like structured composite

In two processes, sandwich-like structural composites of NiS_2@rGO/PPy have been synthesized. The influence of component proportions on the performance of EMW absorption has been investigated. The compound containing 60 mg NiS_2@rGO binary composite exhibited excellent EMW attenuation properties. With a thickness of 2.00–3.50 mm, this novel NiS_2@rGO/PPy sandwich-like composite exhibit an effective EMW absorption bandwidth (RL 10 dB) of 10.96 GHz

(7.04–18.00 GHz). At 16.44 GHz, the best reflection loss is -58.7 dB for a 2.03 mm thick sample containing 6% NiS_2@rGO/PPy. The novel sandwich-like shape, along with various relaxations and interfacial polarization processes, results in superior impedance-matching compatibility. Thus, the NiS_2@rGO/PPy composites exhibit a high absorption capacity, a broad absorption bandwidth, and a thin thickness, making them highly applicable to electromagnetic wave pollution reduction. [62],[63]

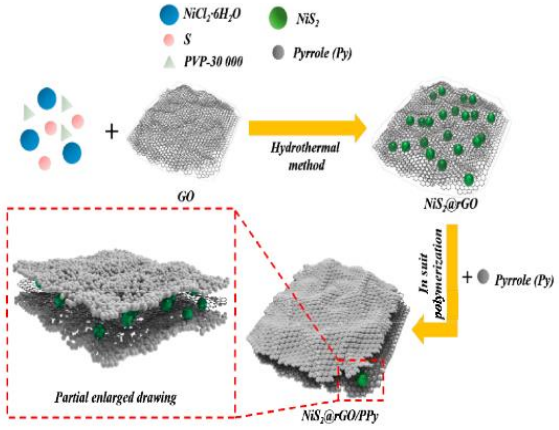

Figure 79. The preparation process of the NiS2@rGO/polypyrrole (PPy) sandwich-like structure composite.

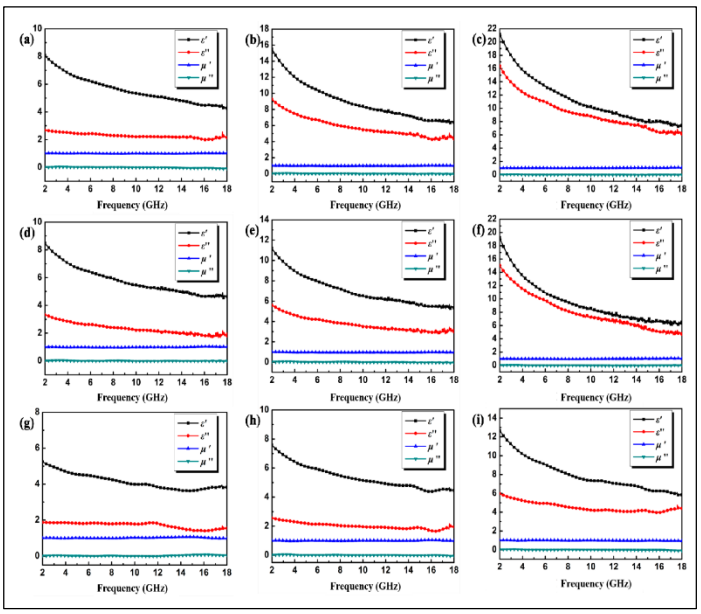

Figure 80. Frequency dependence of the ε', ε", μ', and μ" values of sample A with filler loadings of 4 (a), 6 (b), and 8 wt% (c); sample B with filler loadings of 4 (d), 6 (e), and 8 wt% (f); and sample C with filler loadings of 4 (g), 6 (h), and 8 wt% (i).

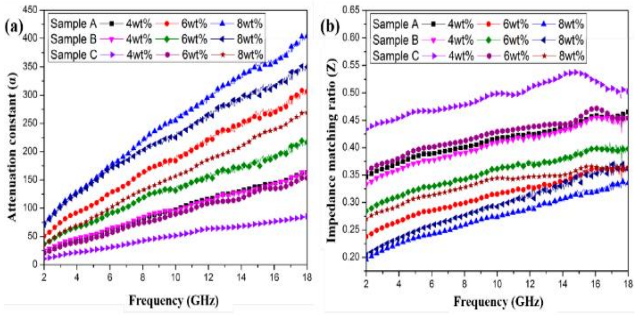

Figure 81. Frequency dependence of the attenuation constant (a) and impedance matching ratio (b) of samples A, B, and C with different filler loading ratios.

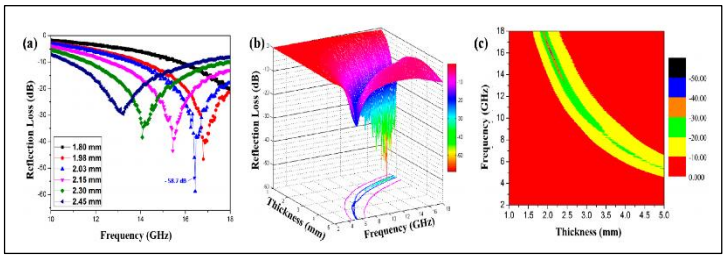

Figure 82. Simulation of reflection loss (RL) curves (a), 3D representations of RL (b), and the corresponding contour map (c) of sample B with a filler loading ratio of 6 wt% in wax composites.

CIP/ABS composites

Achieving tunable structural electromagnetic wave (EMW) absorption qualities using 3D printing technology has proven convenient and effective. This work has been used melt-mixing to create functional carbonyl iron powder/Acrylonitrile-Butadiene-Styrene copolymer (ABS) composites with varying CIP concentrations for 3D printing applications using fused deposition modeling (FDM). According to the ideal impedance matching test, a CIP/ABS composite with a 40% CIP component has the lowest reflection loss (RL). The efficient dispersion of the CIPs in the ABS matrix give these composite excellent mechanical characteristics. The tensile and flexural modulus are higher than pure ABS, while the tensile strength is similar. In addition to its remarkable EMW absorbing and mechanical qualities, the CIP/ABS composite offers tremendous promise for the development of structural absorbers using FDM 3D printing technology, thanks to its 40% CIP component. CIP/ABS composites' EMW absorption characteristics improve as CIP content increases. This is due to the huge attenuation constant, these composites have the lowest RL (-48.71 dB) of all the composites tested (based on optimal impedance matching). For best mechanical properties, the composites with a 40% CIP content in the ABS matrix has been chosen. By preventing molecular chain mobility, CIP particles have operated as physical crosslinking locations. Under external load, however, the material's CIP particles has been able to pin the cracks produced. The tensile and flexural modulus is higher than pure ABS by 32% and 37%, respectively. To produce structural absorbers using FDM 3D printing technology, here proved that a CIP/ABS composite with 40% CIP content could achieve

significant EMW-absorbing performance and outstanding mechanical properties. [64]

Table 27. Basic properties and electromagnetic parameters of BD-MZ-1 carbonyl iron powders (CIPs).

Particle Sizes(μm)	Tap Density (g/cm3)	Electromagnetic Parameters(Part of Frequencies)				
		Frequency (GHz)	εj	ε”	μj	μ”
<10	2.6–3.1	2	20.75	0.43	5.10	2.24
		8	19.46	0.18	2.12	2.59
		18	20.88	0.66	0.65	1.52

Table 28. Sample Description of CIP/ acrylonitrile-butadiene-styrene copolymer (ABS) composites

Samples	ABS (wt.%)	CIPs (wt.%)
Pure ABS	100	0
C-10	90	10
C-20	80	20
C-30	70	30
C-40	60	40
C-50	50	50
C-60	40	60

Table 29. EMW absorption properties of samples C-10, C-20, C-30, C-40, C-50, and C-60. EAB: effective absorption bandwidth

Samples	RL-Min (dB)	EAB-Max (RL<−10 dB, GHz)
C-10	−7.13	0
C-20	−18.37	1.8
C-30	−17.59	2.6
C-40	−48.71	3.3
C-50	−28.99	4.1
C-60	−16.87	4.6

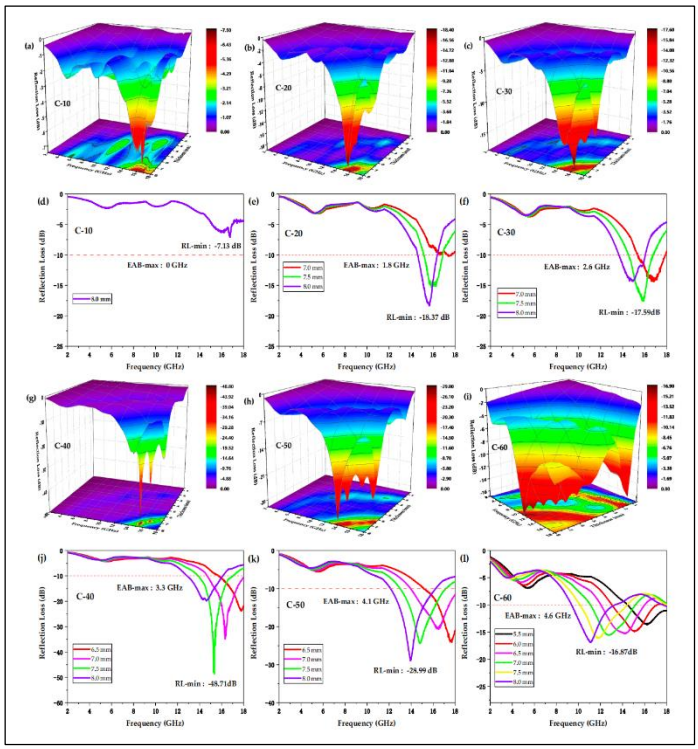

Figure 83. 3D theoretically calculated reflection loss (RL) spectra of CIP/ABS composites with varying CIP contents when the thickness increased from 0.5 mm to 8 mm, and the corresponding 2D RL plots. (a,d): sample C-10. (b,e): sample C-20. (c,f): sample C-30. (g,j): sample C-40. (h,k): sample C-50. (i) and (l): sample C-60.

3) Contrast and the study gap

The widespread development and usage of electronic and electrical equipment in the twenty-first century has resulted in the emergence of a new type of issue known as electromagnetic interference (EMI) [65]. Shielding or absorbing the electromagnetic field is considered while developing an acceptable solution for the EMI problem. Historically, shielding techniques were largely focused on metals and their composites. When doped with particular charge carriers, organic polymers with an extended conjugated system exhibit semiconductor conductivity. The conductivity of the polymers may be modified to meet the requirements of a particular application[66]. It is noted that the materials' strong conductivity and dielectric constant contribute to their great EMI shielding efficiency (SE). As a result, conductive polymers are used in EMI shielding technologies. Due to their benefits over intrinsic ferrites in terms of lightweight, cheap cost, design flexibility, and microwave characteristics, polymer composite materials are suitable as microwave absorbers and EMA materials. Previous research has focused on the creation of polymer composites with EMA characteristics [23]. When we look at the differences between domestic and international research, we can observe that there is a great deal of competitiveness and rapid development of methodologies for designing polymer composite materials.

4) Study the gap of the absorption capacity of GFRP Composite Materials for Electromagnetic Waves

Polymeric materials are commonly employed in engineering applications that demand substantially lightweight structural solutions. Polymeric materials are created to meet specific physical requirements using composite material production processes. Medical, aerospace, automotive, sports goods, maritime purposes, consumer items, architecture, and a variety of civil applications are all typical uses for GFRP composites. The most extensively utilized strategy for improving mechanical performance in terms of specific strength, toughness, and damping capacity is fiber reinforcement. Glass fibers are frequently utilized as reinforcement in polymer matrix composites (PMC) [67]. In comparison to alternative types of reinforcement, glass fibers provide significant benefits in terms of handling and cost. Glass fibers may be employed in GFRP manufacture in two forms: discontinuous as chopped-strand fibers or continuous as glass fiber woven textiles. Glass fiber woven fabric plies are employed in the fabrication of multilayered GFRP composites. Multilayered GFRP composites have anisotropic mechanical characteristics, which may be customized by weaving texture, fiber orientation, and/or load-bearing fiber density. Examples of glass fiber woven fabric texturing are shown below.

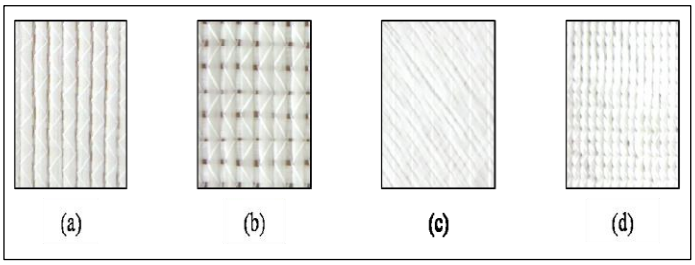

Figure 84. Uniaxial (a), ± 90 biaxial (b), ±45 biaxial (c), and quadriaxial (d) weaving textures in glass fiber woven fabrics.

Table 30. Glass fiber types and designations

Letter Designation	Property or Characteristic
E, electrical	Low electrical conductivity
S, strength	High strength
C, chemical	High chemical durability
M, modulus	High stiffness
An alkali	High alkali or soda-lime glass
D, dielectric	Low dielectric constant

Electrical and magnetic alterations to the polymer matrix and/or glass fiber reinforcements can be used to incorporate electromagnetic wave absorption into PMC composite materials.

Additionally, cascaded surface-modified glass fiber reinforcement layers have been used to increase the inherent impedance. proposed a similar strategy based on three multilayer group layouts for optimal EM wave absorption.

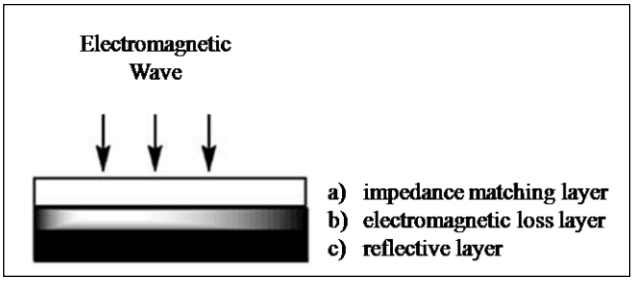

Figure 85. Three-layer group arrangement in effective EM wave absorption

The first layer offers impedance matching at the material-air interface in this configuration. The usage of such layers minimizes reflection loss from the material's surface. These receiving layers should exhibit reduced reflection loss in addition to providing impedance matching. The incident electromagnetic wave's power should be converted to absorption loss by the second stage layers. The effect of reflection loss from these layers should be minimized by adjusting the first layer's impedance. The final stage layers of a multilayered construction should have a high level of reflection to avoid transmission loss. Reflection created by reflection layers should be reabsorbed by lossy layers throughout the reflection route.

5) Post opinion

Now people are aware that the EMI environment and pollution are harmful to their health and degrade the quality of our lives. Thus, the development of a variety of materials that can eliminate or absorb electromagnetic (EM) waves effectively becomes urgent and reduces the harmful EMI. To overcome this problem, the designing and fabrication of EM absorbers are a very important subject in modern society. As a kind of typical EM absorbers, magnetic and dielectric polymer composite materials are required to fulfill the characteristics of abundant resource, low cost, easy preparation, lightweight, relatively low density, high efficiency, and frequency range response.[24]. To maximize electromagnetic absorption, numerous critical factors must be considered, including filler type, loading amount, polymer matrix type, physical thickness, particle sizes, layers, bandwidth, and so on. As such, this study discusses the mechanics of electromagnetic wave absorption of polymer composite materials and discusses the characteristics that improve absorption efficacy.

C. Trend prediction

The widespread development and usage of electronic and electrical equipment in the twenty-first century has resulted in the emergence of a new type of issue known as electromagnetic

interference (EMI). Shielding or absorbing the electromagnetic field is considered while developing an acceptable solution for the EMI problem. Historically, shielding techniques were largely focused on metals and their composites. When doped with particular charge carriers, organic polymers with an extended conjugated system exhibit semiconductor conductivity. The conductivity of the polymers may be modified to meet the requirements of a particular application. It is noted that the materials' strong conductivity and dielectric constant contribute to their great EMI shielding efficiency (SE). As a result, conductive polymers are used in EMI shielding/absorbing technologies. Due to their benefits over intrinsic ferrites in terms of lightweight, cheap cost, design flexibility, and microwave characteristics, polymer composite materials are suitable as microwave absorbers and EMA materials. Previous research has focused on the creation of polymer composites with EMA characteristics. With the advancement of computational technology, there is a bright future for designing EMWA polymer composite materials. Soon, new polymer composite materials design processes and attributes will be introduced to the field. [65],[66].

Further improvements in the EM wave absorption behavior of multilayered structures can be achieved using computational methods. Necessary changes in the extent of the surface modifications along with the arrangements and number of individual layers in the multilayered structures can be previewed by the application of the computation method to further enhance reflection, transmission, and absorption characteristics. For example, the development of the symmetry of the absorption characteristic for the four-layered systems can be predicted by the insertion of additional surface-modified layers in inverse order. Electromagnetic characterization of obtained eight layered structures can be conducted by the presented computation method. In practice, experimental characterization of such a structure by free space is rather a time taking and demanding. Consequently, to overcome such practical limitations effect of additional surface-modified layers on the overall EM wave transmission/reflection characteristic of the multilayered structures can be monitored via computations.

III. Conclusions and Outlook

The conclusions and outlook of this review highlighted the recent developments related to polymer-based composites as promising EM absorbing materials. Summary of all polymer based composite materials for electromagnetic wave absorption covered by this study. The introduction will discuss the study's direction and the current state of history. The next chapter describes electromagnetic wave absorption fundamental theories. It includes the EM spectrum, EM absorption process (reflection and hysteresis), residual loss, loss of dielectric strength, conductance, and relaxation. Complex permittivity and permeability, conductivity, nanotechnology, skin depth, impedance, and the free-space method.

Then we'll look at international and domestic research progress, and how that work has been done in recent years as a summary of polymer composites and all the materials below have electromagnetic absorption properties studied. The first step is material Constructing Polyaniline Composites as Microwave Absorbers from aniline and emulsion-grade polyvinyl chloride. then Nanocrystalline FeCuNbSiB alloy flakes/polymer composite sheets with variable flake thicknesses. A thinned magnetic alloy flakes/polymer composite sheet was examined for its electromagnetic wave absorption characteristics. And also Mechanical grinding of MWCNT-filled epoxy composites with PMMA coatings

The use of carbon microcoil-polyurethane composites to filter electromagnetic radiation. CMC-polyurethane composites have been made by dispersing CMCs in PU using dimethylformamide. EM-absorbing magnetite carbon nanofiber composite is presented here. Efficient Magnetic Absorption using Sandwich-Like rGO/CuS/Polypyrrole Nanoarchitectures and Using emulsion polymerization, a conducting polymer composite with barium ferrite nanoparticles review given.

In situ polymerization has been used to create thermally conductive thermoplastic nanocomposites by combining PANI-coated MWNTs with PMMA. Microwave absorption properties of Fe_3O_4@SiO_2 [68] composites and Compounds of carbonyl iron and polychloroprene are described. Activated Carbon Powder Composites for EM Shielding have been presented. The CNTs/$BaTiO_3$/PANI or CBP ternary composites have been synthesized by sol-gel in situ polymerization and Poly (3,4-ethylene dioxythiophene) Composite Graphene Sheets Using a special silica fabric and a freeze-drying process, on the other hand, a simple one-pot polyreaction has been produced 3-dimensional reticulated -Fe_2O_3/PPy hybrids. [69]

Polyaniline nanofibers have been chemically polymerized to make millimeter-wave absorber fabrics. In W-type hexaferrite powder polymer composites, the influence of an SL/ FSS on the absorption properties of grounded ferrite composites is investigated. Conjugated polymers, Carbonyl Iron/MnZn Ferrite/PVC composites and self-healing electromagnetism (p(HEMAcoBA)-Fe_3O_4), and functional monomers (Fc/CD-Fe_3O_4 complexes) are presented.

Nanosized Conducting Black-Silicone Rubber Composites, Microwave Absorbing Epoxy Resin Composites, X-band Coconut Fiber Coir, and Charcoal Powder for EM Absorption have presented. Fe_3O_4/PANI composites, Polyvinylpyrrolidone-TiO_2/polyacrylonitrile-SiO_2 nanocomposites, Stealth polymer matrix composite, Graphene nanoplatelet composite films, High Microwave Absorption Sandwich Composite, Polypyrrole nanocomposite, CIP/ABS polymer composites and their EMW absorption properties have been discussed here.

A List of Tables

Table 1. Dielectric properties of 1:1.5 Pani: PVC composite at S,C,X bands[14]

Table 2. Absorption coefficient and skin depth of PANI : PVC composite at S band (at 2.97 GHz).[14]

Table 3. EMI SE of coated (PMMA/ 25 wt% CNTs) and uncoated samples in the 100 MHz - 14GHz frequency range[3]

B List of Figures

Figure 17. The variation of shielding effectiveness relative to the different composition ratios of the CMCs in the CMC-PU-DMF mixture[19].

Figure 18. The dependence of the PU-CMC sheet volume resistivity relative to the number of coatings[19].

Figure 19. The variation of shielding effectiveness for sample B relative to the different thicknesses of the coated layers[19].

Figure 20. (a) Total electromagnetic shielding efficiency, SET, for composites CNF10 and CNF:Mag20. Reflection shielding, SER (Dot), absorption shielding, SEA (Dash), transmission shielding, SET (line). The thickness of specimens: 13 mm. (b) Absorption coefficients for CNF (dashes), CNF:Mag (lines) composites with compositions indicated in the inset. (c) Absorbed, reflected and (d) transmitted power of CNF10 (dash) and CNF:Mag20 (line)[20].

Figure 21. (Color online) Variation in the EMI shielding effectiveness, SEA and SER of polyaniline composites having different weight ratios of barium ferrite: PBF21, PBF11, PBF12, and PBF13, with frequency[23].

Figure 22. The reflection loss values of the Fe3O4@SiO2core–shell polyaniline-based composites with various sample thickness and (a) 0 wt%, (b) 2 wt%, (c) 4 wt%, (d) 6 wt%Fe3O4@SiO2 core–shell fillers[24].

Figure 23. The Fe3O4@SiO2 core–shell polyaniline-based composites. (a) The 2D map colour filling patterns of RL characteristics with various sample thickness, (b) the dependence off$_{up}$,f$_{low}$ and W=f$_{up}$/f$_{low}$ on thickness t and (c) reflection characteristics at the optimum thickness tm for 4 wt% Fe3O4@SiO2 core–shell fillers. (d) Eddy current loss (Co) curve of 0 wt%, 2 wt%, 4 wt%, 6 wt% Fe3O4@SiO2 core–shell fillers[24]

Figure 24. Structure of proposed double-layer microwave absorbing material layers[26],

Figure 25. Schematic representation of the preparation of functional cotton and nylon fabrics based on polyaniline nanofibers and their composite[27].

Figure 26. Transmission electron microscope of (a)graphite, (b) polyaniline nanofibers (P) and (c) polyaniline nanofiber graphite composite (GpP) and (d) solid-state ultraviolet–visible spectra of polyaniline nanofibers and their graphite composite[27].

Figure 27. Variation of EMI SE, SEA and SER of (a) polyaniline nanofibers (P) and (b) polyaniline nanofiber graphite composite (GpP) of thickness 1 mm in the 8.2–18 GHz frequency range[27].

Figure 28. Reflection loss determined in the grounded ferrite composites with various layer thicknesses[29]

Figure 29. Complex permeability and permittivity of rubber composite containing CoZnW hexaferrite powders[29]

Figure 30. Reflection loss determined in the composite structure, implemented with SL-FSS on a grounded ferrite composite (thickness = 2.9 mm), with increasing SL-FSS resistance (R)[29]

Figure 31. Frequency dependences of real and imaginary parts of complex (relative) permeability for prepared CI/MnZn/PVC composites with different filler volume ratios[32].

Figure 32. Frequency dependences of return loss for prepared CI/MnZn/PVC composites with different filler volume ratios[32].

Figure 33. Complex permittivity vs. frequency. (a) Real part (ε'). (b) Imaginary part (ε''). (c) Dielectric loss tangent (tan δ_{ε})[33]

Figure 34. Reflection loss (RL) vs. frequency (a) RL of samples S_0–S_3 at thickness 2mm (b) RL of sample S_2 at different thicknesses[33].

Figure 35. (a) Normalized impedance vs. frequency of all samples at thickness 2mm. (b) Schematic of RL phenomenon of a single layer MW absorber[33].

Figure 36. Schematic drawings for the preparation of reduced graphene oxide paper and powder by using the spaced method in a soxhlet unit. GO, Graphite Oxide; rGO, reduced GO[4].

Figure 37. Relative permittivity for the epoxy, the hardener, and the cured epoxy at the X-band frequency[4]

Figure 38. The frequency dependence of (a) The real part of permittivity (ε'), (b) The imaginary part of permittivity (ε"), and (c) The tangent loss (tanδ) at various rGO loadings[4].

Figure 39. SE_A and SE_R of PVP–TiO2/PAN–SiO2 nanofibre nanocomposites that were synthesized with (a) 0.3, (b) 0.4 and (c)0.5mlh^{-1} flow rates[36].

Figure 40. Test methods for electromagnetic evaluation of Radar absorbing materials. (a) Waveguide. (b) Free space. (c) Open range RCS measurements. [Color figure can be viewed at wileyonlinelibrary.com][38]

Figure 41. DC conductivity as a function of GRNP's content in PANI at 100 °C (PANI-GRNP's and p-TSA doped PANI-GRNP's composite)[39].

Figure 42. Absorption coefficient as a function of frequency for PANI and PANI- GRNP's composite in X-band[39].

Figure 43. Reflection coefficient as a function of frequency for PANI and PANI- GRNP's composite in X-band[39].

Figure 44. EMI-SE as a function of frequency for PANI and PANI-GRNP's com- posite in X-band[39].

Figure 45. Skin depth as a function of frequency for PANI and PANI-GRNP's composite in X-band[39].

Figure 46. Variation of dielectric constant as a function of frequency for PANI and PANI-GRNP's composite in X-band[39].

Figure 47. Variation of dielectric loss as a function of frequency for PANI and PANI-GRNP's composite in X-band[39]

Figure 48. Variation of the real part of magnetic permeability as a function of frequency for PANI and PANI-GRNP's composite in X-band[39].

Figure 49. Variation of the imaginary part of magnetic permeability as a function of frequency for PANI and PANI-GRNP's composite in X-band[39].

Figure 50. The schematic diagram for the synthesis of polypyrrole-barium ferrite-tantalum pentoxide (PPY/BF/TO) composite[40].

Figure 51. Variation of shielding effectiveness due to (a) absorption, (b) reflection, of polypyrrole/barium ferrite/tantalum oxide composites with frequency[40]

Figure 52. The behavior of (a) real (ε'), (b) imaginary (ε'') parts of complex permittivity of PPy nanocomposites as a function of frequency. (c) Dependence of real (μ′) and (d) imaginary (μ″) parts of magnetic permeability nanocomposites on frequency[40].

Figure 53. Variation of (a) dielectric tangent loss (b) magnetic tangent loss with frequency[40].

Figure 54. (a) The real and (b) imaginary parts of the permittivity of the samples; (c) the real and (d) imaginary parts of the permeability of the samples; (e) dielectric and (f) magnetic loss tangent of the samples[43].

Figure 55. Reflection loss curves of(a) rGO/p-Fe3O4(1:20)@PANI, (b) rGO/p-Fe3O4(1:10)@PANI, (c) rGO/p-Fe3O4(1:5)@PANI, (d) rGO/p-Fe3O4(1:5) samples with different thicknesses[43].

Figure 56. (a) Imaginary impedance and (b) real impedance of complex impedance Z_{in} ofthe samples[43].

Figure 57. Attenuation constant of α of the samples[43]

Figure 58. Complex permittivity and permeability of rGO/CuS/PPy with the filler loading of 5 wt.% (a), 10 wt.% (b), 15 wt.% (c), and 20 wt.% (d)[44].

Figure 59. RL curves of paraffin composites containing 5 wt.% (a), 10 wt.% (b), 15 wt.% (c), and 20 wt.% (d) of rGO/CuS/PPy[44].

Figure 60. The preparation process of composites film[48]

Figure 61. Schematic diagram of the composite film dried apparatus with a static magnetic field produced by electromagnetic induction coils[48].

Figure 62. The relative complex permittivity and permeability of carbonyl iron-paraffin wax composites vs frequency[48].

Figure 63. The reflection loss of calculation and films preparation with and without external magnetic field[48]

Figure 64. EMI shielding effectiveness (a) and absorption (b) of the four composites[51].

Figure 65. Electromagnetic wave absorbing mechanism of CBP composite[52].

Figure 66. Complex permeability of samples: (a) real part and (b) imaginary part[52].

Figure 67. (a) Reflection loss of samples with the thickness of 4mm and (b) reflection loss ofCBP3 with different thicknesses[52].

Figure 68. a Schematic illustration of GNs-PEDOT. b FTIR spectra of GNs-PEDOT. c Raman spectra of GO and GNs-PEDOT[54]

Figure 69. The complex relative permittivity (a), permeability (b), and loss tangent (c) of GNs-PEDOT. Reflection loss curves of d GNs, e PEDOT, and f GNs-PEDOT[54]

Figure 70. Scheme of the procedures for RGO/silica textile/PF composites[55].

Figure 71. Real (a), imaginary permittivity (b) and tangent loss (c) of the samples marked; Real (e), imaginary permittivity (e) and tangent loss (f) at various frequencies[55]

Figure 72. The frequency dependence of dielectric properties for the paraffin-based composites (10 wt%): (a) real permittivity; (b) imaginary permittivity; (c) conductivity fitted by Debye theory and (d) cole-cole plots[57].

Figure 73. Three-dimensional plots of RL values for paraffin-based composites: (a) S-1, (b) S-2 and (c) S-3; EA performance comparison of three samples: (d) absorption peaks, (e) RL ≤ −10 dB peak width and (f) RL ≤ −20 dB peak width[57]

Figure 74. Numerical calculated optimum thickness (a) of S-2 for minimum RL at expected frequency; optimum thickness and EA performance at corresponding thickness (b)[57].

Figure 75. Self-healing of microwave absorptive properties of p(HEMA-co-BA)-Fe3O4 coating. A) 3 mm; B) 4 mm; C) 5 mm[58].

Figure 76. A–D) Self-healing behavior of p(HEMA-co-BA)-Fe3O4 coating. LSCM photos of coating with one

crack on the surface (A, C) before and (B, D) after healing. E–F) SEM photos of coating with one crack on the surface (E) before and (F) after healing[58].

Figure 77. The evaluation models of (a) conventional electromagnetic interference (EMI) shielding and (b) microwave absorption. MAM: microwave-absorbing material[59].

Figure 78. Fe3O4@polyaniline yolk-shell micro/nanospheres synthesized by a facile silica-assisted solution phase method[60]

Figure 79. The preparation process of the NiS2@rGO/polypyrrole (PPy) sandwich-like structure composite[62].

Figure 80. Frequency dependence of the ε', ε", μ', and μ" values of sample A with filler loadings of 4 (a), 6 (b), and 8 wt% (c); sample B with filler loadings of 4 (d), 6 (e), and 8 wt% (f); and sample C with filler loadings of 4 (g), 6 (h), and 8 wt% (i).[62]

Figure 81. Frequency dependence of the attenuation constant (a) and impedance matching ratio (b) of samples A, B, and C with different filler loading ratios[62].

Figure 82. Simulation of reflection loss (RL) curves (a), 3D representations of RL (b) and the corresponding contour map (c) of sample B with a filler loading ratio of 6 wt% in wax composites[62].

Figure 83. 3D theoretically calculated reflection loss (RL) spectra of CIP/ABS composites with varying CIP contents when the thickness increased from 0.5 mm to 8 mm, and the corresponding 2D RL plots. (a,d): sample C-10. (b,e): sample C-20. (c,f): sample C-30. (g,j): sample C-40. (h,k): sample C-50. (i) and (l): sample C-60.[64]

Figure 84. Uniaxial (a), ± 90 biaxial (b), ±45 biaxial (c), and quadriaxial (d) weaving textures in glass fiber woven fabrics[1].

Figure 85. Three-layer group arrangement in effective EM wave absorption[1]

CONFLICT OF INTEREST

The authors declare no conflict of interests.

REFERENCES

[1] G. Gurer, "Design and Characterization of Electromagnetic Wave," no. September, 2010.

[2] R. K. Jani, L. Saini, and S. R. Vadera, "Size dependent percolation threshold and microwave absorption properties in nano carbon black/silicon rubber composites," J. Appl. Phys., vol. 131, no. 4, 2022, doi: 10.1063/5.0071517.

[3] A. S. Hoang, H. N. Nguyen, H. T. Bui, A. T. Tran, V. A. Duong, and V. B. Nguyen, "Carbon nanotubes materials and their application to guarantee safety from exposure to electromagnetic fields," Adv. Nat. Sci. Nanosci. Nanotechnol., vol. 4, no. 2, 2013, doi: 10.1088/2043-6262/4/2/025012.

[4] A. F. Ahmad et al., "Preparation of a chemically reduced graphene oxide reinforced epoxy resin polymer as a composite for electromagnetic interference shielding and microwave-absorbing applications," Polymers (Basel)., vol. 10, no. 11, 2018, doi: 10.3390/polym10111180.

[5] J. Huo, L. Wang, and H. Yu, "Polymeric nanocomposites for electromagnetic wave absorption," J. Mater. Sci., vol. 44, no. 15, pp. 3917–3927, 2009, doi: 10.1007/s10853-009-3561-1.

[6] W. Liu et al., "Composition Design and Structural Characterization of MOF-Derived Composites with Controllable Electromagnetic Properties," ACS Sustain. Chem. Eng., vol. 5, no. 9, 2017, doi: 10.1021/acssuschemeng.7b01514.

[7] R. Zhao and G. Zhao, "Electromagnetic Wave Absorption Polymer Nanocomposites," in Reference Module in Materials Science and Materials Engineering, 2021. doi: 10.1016/b978-0-12-820352-1.00184-x.

[8] X. Yan et al., "Electromagnetic Interference Shielding Polymer Nanocomposites," in Multifunctional Nanocomposites for Energy and Environmental Applications, 2018. doi: 10.1002/9783527342501.ch19.

[9] D. K. Setua, B. Mordina, A. K. Srivastava, D. Roy, and N. Eswara Prasad, "Carbon nanofibers-reinforced polymer nanocomposites as efficient microwave absorber," in Fiber-Reinforced Nanocomposites: Fundamentals and Applications, 2020. doi: 10.1016/b978-0-12-819904-6.00018-9.

[10] L. Lyu et al., "An overview of electrically conductive polymer nanocomposites toward electromagnetic interference shielding," Engineered Science, vol. 2. 2018. doi: 10.30919/es8d615.

[11] J. Yan et al., "Polypyrrole-Based Composite Materials for Electromagnetic Wave Absorption," Polymer Reviews, vol. 61, no. 3. 2021. doi: 10.1080/15583724.2020.1870490.

[12] M. Verma, A. P. Singh, P. Sambyal, B. P. Singh, S. K. Dhawan, and V. Choudhary, "Barium ferrite decorated reduced graphene oxide nanocomposite for effective electromagnetic interference shielding," Phys. Chem. Chem. Phys., vol. 17, no. 3, 2015, doi: 10.1039/c4cp04284k.

[13] N. F. N. Yah, H. A. Rahim, Y. S. Lee, F. H. Wee, and H. H. Zainal, "Electromagnetic wave absorption properties of novel green composites coconut fiber coir and charcoal powder over X-band frequency for electromagnetic wave absorbing applications," Adv. Electromagn., vol. 7, no. 1, pp. 13–18, 2018, doi: 10.7716/aem.v7i1.598.

[14] "Conducting Polyaniline Composites as Microwave Absorbers.," Publ. online Wiley Intersci. (www.interscience.wiley.com)., p. 5, 2007, [Online]. Available: https://scholar.google.com/scholar?q=1.+Conducting+Polyaniline+Composites+as+Microwave+Absorbers.+Conducting+Polyaniline+Composites+as+Microwave+Absorbers&hl=en&as_sdt=0&as_vis=1&oi=scholart

[15] S. Naghdi et al., "Graphene family, and their hybrid structures for electromagnetic interference shielding applications: Recent trends and prospects," Journal of Alloys and Compounds, vol. 900. 2022. doi: 10.1016/j.jallcom.2021.163176.

[16] M. Qiao, X. Lei, Y. Ma, L. Tian, K. Su, and Q. Zhang, "Well-Defined Core-Shell Fe3O4@Polypyrrole Composite Microspheres with Tunable Shell Thickness: Synthesis and Their Superior Microwave Absorption Performance in the Ku Band," Ind. Eng. Chem. Res., vol. 55, no. 22, 2016, doi: 10.1021/acs.iecr.5b04814.

[17] T. G. Lee, J. B. Kim, and T. H. Noh, "Electromagnetic wave absorption characteristics of nanocrystalline FeCuNbSiB alloy flakes/polymer composite sheets with different flake thickness," J. Magn., vol. 14, no. 4, pp. 155–160, 2009, doi: 10.4283/JMAG.2009.14.4.155.

[18] W. J. Lee and C. G. Kim, "Electromagnetic wave absorbing composites with a square patterned conducting polymer layer for wideband characteristics," Shock Vib., vol. 2014, 2014, doi: 10.1155/2014/318380.

[19] G. H. Kang and S. H. Kim, "Electromagnetic wave shielding effectiveness based on carbon microcoil-polyurethane composites," J. Nanomater., vol. 2014, 2014, doi: 10.1155/2014/727024.

[20] M. Crespo, N. Méndez, M. González, J. Baselga, and J. Pozuelo, "Synergistic effect of magnetite nanoparticles and carbon nanofibres in electromagnetic absorbing composites," Carbon N. Y., vol. 74, pp. 63–72, 2014, doi: 10.1016/j.carbon.2014.02.082.

[21] L. L. Vovchenko et al., “Dielectric and microwave shielding properties of three-phase composites graphite nanoplatelets/carbonyl iron/epoxy resin,” Appl. Nanosci., vol. 10, no. 12, 2020, doi: 10.1007/s13204-020-01326-w.

[22] P. Kumar, U. Narayan Maiti, A. Sikdar, T. Kumar Das, A. Kumar, and V. Sudarsan, “Recent Advances in Polymer and Polymer Composites for Electromagnetic Interference Shielding: Review and Future Prospects,” Polymer Reviews, vol. 59, no. 4. 2019. doi: 10.1080/15583724.2019.1625058.

[23] A. Ohlan, K. Singh, A. Chandra, and S. K. Dhawan, “Microwave absorption properties of conducting polymer composite with barium ferrite nanoparticles in 12.4-18 GHz,” Appl. Phys. Lett., vol. 93, no. 5, pp. 18–21, 2008, doi: 10.1063/1.2969400.

[24] C. Journal and O. F. Chinese, “介 孔 SiO 2 / Fe 3 O 4 中空磁性微球的漆酶固定化 (,” vol. 34, pp. 2–8, 2013.

[25] N. Janem, Z. S. Azizi, and M. M. Tehranchi, “Microwave absorption and magnetic properties of thin-film Fe3O4 @polypyrrole nanocomposites: The synthesis method effect,” Synth. Met., vol. 282, 2021, doi: 10.1016/j.synthmet.2021.116948.

[26] F. M. Idris, M. Hashim, Z. Abbas, I. Ismail, R. Nazlan, and I. R. Ibrahim, “Recent developments of smart electromagnetic absorbers based polymer-composites at gigahertz frequencies,” J. Magn. Magn. Mater., vol. 405, pp. 197–208, 2016, doi: 10.1016/j.jmmm.2015.12.070.

[27] N. Joseph, J. Varghese, and M. T. Sebastian, “In situ polymerized polyaniline nanofiber-based functional cotton and nylon fabrics as millimeter-wave absorbers,” Polym. J., vol. 49, no. 4, pp. 391–399, 2017, doi: 10.1038/pj.2016.121.

[28] S. K. Srivastava and V. Mittal, “Advanced Nanostructured Materials in Electromagnetic Interference Shielding,” in Hybrid Nanomaterials, 2017. doi: 10.1002/9781119160380.ch5.

[29] H. S. Cho and S. S. Kim, “Improvement of Microwave Absorbance of Polymer Composites of W-Type Hexaferrite Powders by Attachment of Frequency Selective Surface,” Arch. Metall. Mater., vol. 62, no. 2, pp. 1325–1328, 2017, doi: 10.1515/amm-2017-0202.

[30] J. H. Lim and S. S. Kim, “Multiple magnetic resonance and microwave absorption of metamaterial absorbers composed of double split ring resonators on grounded carbonyl iron composites,” AIP Adv., vol. 7, no. 12, 2017, doi: 10.1063/1.5013164.

[31] A. Yadav, R. Kumar, and B. Sahoo, “Graphene Oxide Coatings on Amino Acid Modified Fe Surfaces for Corrosion Inhibition,” ACS Appl. Nano Mater., vol. 3, no. 4, 2020, doi: 10.1021/acsanm.0c00243.

[32] R. Dosoudil and M. Ušáková, “High-frequency absorbing performances of carbonyl iron/MnZn Ferrite/PVC polymer composites,” Acta Phys. Pol. A, vol. 131, no. 4, pp. 687–689, 2017, doi: 10.12693/APhysPolA.131.687.

[33] R. K. Jani, M. K. Patra, L. Saini, A. Shukla, C. P. Singh, and S. R. Vadera, “Tuning of microwave absorption properties and electromagnetic interference (EMI) shielding effectiveness of nanosize conducting black-silicone rubber composites over 8–18 GHz,” Prog. Electromagn. Res. M, vol. 58, no. May, pp. 193–204, 2017, doi: 10.2528/PIERM17022704.

[34] X. Liu et al., “Enhanced Microwave Absorption Properties by Tuning Cation Deficiency of Perovskite Oxides of Two-Dimensional LaFeO3/C Composite in X-Band,” ACS Appl. Mater. Interfaces, vol. 9, no. 8, 2017, doi: 10.1021/acsami.6b15379.

[35] Y. Yang, M. C. Gupta, K. L. Dudley, and R. W. Lawrence, “Conductive carbon nanofiber-polymer foam structures,” Adv. Mater., vol. 17, no. 16, 2005, doi: 10.1002/adma.200500615.

[36] O. Nakhaei, N. Shahtahmassebi, M. R. Roknabadi, and M. Behdani, “Synthesis, UV-shielding and electromagnetic wave absorbing properties of polyvinylpyrrolidone-TiO2/polyacrylonitrile-SiO2 nanofibre nanocomposites,” Bull. Mater. Sci., vol. 42, no. 1, pp. 3–10, 2019, doi: 10.1007/s12034-019-1734-3.

[37] S. T. Hsiao et al., “Lightweight and flexible reduced graphene oxide/water-borne polyurethane composites with high electrical conductivity and excellent electromagnetic interference shielding performance,” ACS Appl. Mater. Interfaces, vol. 6, no. 13, 2014, doi: 10.1021/am502412q.

[38] C. G. Jayalakshmi, A. Inamdar, A. Anand, and B. Kandasubramanian, “Polymer matrix composites as broadband radar absorbing structures for stealth aircrafts,” J. Appl. Polym. Sci., vol. 136, no. 14, pp. 1–21, 2019, doi: 10.1002/app.47241.

[39] S. Khasim, “Polyaniline-Graphene nanoplatelet composite films with improved conductivity for high performance X-band microwave shielding applications,” Results Phys., vol. 12, no. December 2018, pp. 1073–1081, 2019, doi: 10.1016/j.rinp.2018.12.087.

[40] P. Gairola, L. P. Purohit, S. P. Gairola, P. Bhardwaj, and S. Kaushik, “Enhanced electromagnetic absorption in ferrite and tantalum pentoxide based polypyrrole nanocomposite,” Prog. Nat. Sci. Mater. Int., vol. 29, no. 2, pp. 170–176, 2019, doi: 10.1016/j.pnsc.2019.03.011.

[41] M. A. Dar, R. K. Kotnala, V. Verma, J. Shah, W. A. Siddiqui, and M. Alam, “High magneto-crystalline anisotropic core-shell structured Mn 0.5Zn 0.5Fe 2O 4/polyaniline nanocomposites prepared by in situ emulsion polymerization,” J. Phys. Chem. C, vol. 116, no. 9, 2012, doi: 10.1021/jp205652d.

[42] R. Manna, K. Ghosh, and S. K. Srivastava, “Functionalized Graphene/Nickel/Polyaniline Ternary Nanocomposites: Fabrication and Application as Electromagnetic Wave Absorbers,” Langmuir, vol. 37, no. 24, 2021, doi: 10.1021/acs.langmuir.1c00804.

[43] H. Cai, B. Cheng, H. Xiao, and Q. Wei, “Synthesis of rGO/p-Fe3O4@PANI three-phase nanomaterials and electromagnetic wave absorption properties,” Mater. Res. Express, vol. 6, no. 12, 2019, doi: 10.1088/2053-1591/ab5727.

[44] * Bing Zhang 1, Shaofeng Lin 2, Jingjing Zhang 2, Xiaopeng Li 2 and Xiaodong Sun 3, “Facile Synthesis of Sandwich-Like rGO/CuS/Polypyrrole Nanoarchitectures for Efficient Electromagnetic Absorption Bing,” Materials (Basel)., vol. 67, no. 1, pp. 421–431, 2006.

[45] J. Ran, L. Shen, L. Zhong, and H. Fu, “Synthesis of Silanized MoS2/Reduced Graphene Oxide for Strong Radar Wave Absorption,” Ind. Eng. Chem. Res., vol. 56, no. 38, 2017, doi: 10.1021/acs.iecr.7b02721.

[46] Y. Liu, Z. Chen, W. Xie, S. Song, Y. Zhang, and L. Dong, “In-Situ Growth and Graphitization Synthesis of Porous Fe 3 O 4 /Carbon Fiber Composites Derived from Biomass as Lightweight Microwave Absorber,” ACS Sustain. Chem. Eng., vol. 7, no. 5, 2019, doi: 10.1021/acssuschemeng.8b06339.

[47] F. Wang, C. Yin, J. Li, X. Wei, L. Cui, and T. Li, “Study on electromagnetic properties of Fe3O4 nanoparticles dispersed in cellulose matrix with core-shell structure,” Integr. Ferroelectr., vol. 163, no. 1, 2015, doi: 10.1080/10584587.2015.1041364.

[48] H. Wang, M. Li, and X. Li, “Influence of external magnetic field on the microwave absorption properties of carbonyl iron and polychloroprene composites film,” AIP Adv., vol. 6, no. 12, 2016, doi: 10.1063/1.4972239.

[49] A. Mandal and C. K. Das, “Effect of BaTiO3 on the microwave absorbing properties of Co-doped Ni-Zn ferrite nanocomposites,” J. Appl. Polym. Sci., vol. 131, no. 4, 2014, doi: 10.1002/app.39926.

[50] C. Xia et al., “Dual-functional natural-fiber reinforced composites by incorporating magnetite,” Compos. Part B Eng., vol. 93, 2016, doi: 10.1016/j.compositesb.2016.03.016.

[51] C. Xia et al., “Scalable fabrication of natural-fiber reinforced composites with electromagnetic interference shielding properties by incorporating powdered activated carbon,” Materials (Basel)., vol. 9, no. 1, pp. 1–9, 2016, doi: 10.3390/ma9010010.

[52] L. Yu, Y. Zhu, C. Qian, Q. Fu, Y. Zhao, and Y. Fu, “Nanostructured Barium Titanate/Carbon Nanotubes Incorporated Polyaniline as Synergistic Electromagnetic Wave Absorbers,” J. Nanomater., vol. 2016, 2016, doi: 10.1155/2016/6032307.

[53] Z. Xu et al., “Pea-like Fe/Fe3C Nanoparticles Embedded in Nitrogen-Doped Carbon Nanotubes with Tunable Dielectric/Magnetic Loss and Efficient Electromagnetic Absorption,” ACS Appl. Mater. Interfaces, vol. 11, no. 4, 2019, doi: 10.1021/acsami.8b19201.

[54] X. Zhang, Y. Huang, and P. Liu, “Enhanced Electromagnetic Wave Absorption Properties of Poly(3,4-ethylenedioxythiophene) Nanofiber-

Decorated Graphene Sheets by Non-covalent Interactions," Nano-Micro Lett., vol. 8, no. 2, pp. 131–136, 2016, doi: 10.1007/s40820-015-0067-z.

[55] W. L. Song et al., "Strong and thermostable polymeric graphene/silica textile for lightweight practical microwave absorption composites," Carbon N. Y., vol. 100, pp. 109–117, 2016, doi: 10.1016/j.carbon.2016.01.002.

[56] F. Wu et al., "Controllable Coating of Polypyrrole on Silicon Carbide Nanowires as a Core-Shell Nanostructure: A Facile Method to Enhance Attenuation Characteristics against Electromagnetic Radiation," ACS Sustain. Chem. Eng., vol. 7, no. 2, 2019, doi: 10.1021/acssuschemeng.8b04676.

[57] W. Jiang, M. Sun, K. Zhang, F. Wu, A. Xie, and M. Wang, "Three-dimensional (3D) α-Fe2O3/polypyrrole (PPy) nanocomposite for effective electromagnetic absorption," AIP Adv., vol. 6, no. 6, 2016, doi: 10.1063/1.4954932.

[58] Y. M. Wang, M. Pan, X. Y. Liang, B. J. Li, and S. Zhang, "Electromagnetic Wave Absorption Coating Material with Self-Healing Properties," Macromol. Rapid Commun., vol. 38, no. 23, pp. 1–8, 2017, doi: 10.1002/marc.201700447.

[59] Y. Wang, Y. Du, P. Xu, R. Qiang, and X. Han, "Recent advances in conjugated polymer-based microwave absorbing materials," Polymers (Basel)., vol. 9, no. 1, 2017, doi: 10.3390/polym9010029.

[60] X. Wang, M. Zhang, J. Zhao, G. Huang, and H. Sun, "Fe 3 O 4 @polyaniline yolk-shell micro/nanospheres as bifunctional materials for lithium storage and electromagnetic wave absorption," Appl. Surf. Sci., vol. 427, pp. 1054–1063, 2018, doi: 10.1016/j.apsusc.2017.09.118.

[61] X. L. Zheng, Z. H. Zhu, and X. M. Li, "The absorbing properties of Fe73.5Cu1Nb 3Si13.5B9 amorphous powder/S-glass fiber-reinforced epoxy composite panels," Rare Met., vol. 32, no. 3, 2013, doi: 10.1007/s12598-013-0035-z.

[62] Z. Zhang et al., "NiS2@rGO nanosheet wrapped with PPy aerogel: A sandwich-like structured composite for excellent microwave absorption," Nanomaterials, vol. 9, no. 6, 2019, doi: 10.3390/nano9060833.

[63] W. Xu, S. Li, W. Zhang, B. Ouyang, W. Yu, and Y. Zhou, "Nitrogen-Doped Ti3C2TxMXene Induced by Plasma Treatment with Enhanced Microwave Absorption Properties," ACS Appl. Mater. Interfaces, vol. 13, no. 41, 2021, doi: 10.1021/acsami.1c17015.

[64] W. Lai, Y. Wang, and J. He, "Effects of carbonyl iron powder (CIP) content on the electromagnetic wave absorption and mechanical properties of CIP/ABS composites," Polymers (Basel)., vol. 12, no. 8, 2020, doi: 10.3390/POLYM12081694.

[65] M. Jaroszewski, S. Thomas, and A. V. Rane, Advanced Materials for Electromagnetic Shielding: Fundamentals, Properties, and Applications. 2018.

[66] Handbook of Advanced Ceramics and Composites. 2020. doi: 10.1007/978-3-030-16347-1.

[67] V. Shukla, "Advances in Hybrid Conducting Polymer Technology for EMI Shielding Materials," in Engineering Materials, 2021. doi: 10.1007/978-3-030-62090-5_9.

[68] Y. Yin, X. Liu, X. Wei, R. Yu, and J. Shui, "Porous CNTs/Co Composite Derived from Zeolitic Imidazolate Framework: A Lightweight, Ultrathin, and Highly Efficient Electromagnetic Wave Absorber," ACS Appl. Mater. Interfaces, vol. 8, no. 50, 2016, doi: 10.1021/acsami.6b12178.

[69] L. Du et al., "Surfactant-assisted solvothermal synthesis of Ba(CoTi)xFe 12-2xO19 nanoparticles and enhancement in microwave absorption properties of polyaniline," J. Phys. Chem. C, vol. 114, no. 46, 2010, doi: 10.1021/jp1067268.

How to cite this article:

W. H. Nishani De Soyza, Alfadil Yousif, Junliang Liu "Polymer Composite Materials for Electromagnetic Waves Absorption" International Journal of Engineering Works, Vol. 11, Issue 04, PP. 61-104, April 2024. https://doi.org/10.34259/ijew.24.110461104.